MAGNETOTELLURIC INVESTIGATIONS OF KILAUEA VOLCANO, HAWAI`I, PART II: NUMERICAL MODELING AND DATA INTERPRETATION

by

G. Michael Hoversten [1]

Erika Gasperikova [1]

Greg A. Newman [2]

James P. Kauahikaua [3]

Michael P. Ryan [4]

Nestor Cuevas [5]

[1] Lawrence Berkeley National Laboratory

[2] Sandia National Laboratories

[3] U.S. Geological Survey
Hawaiian Volcano Observatory

4 U.S. Geological Survey
National Center, Reston Virginia

[5] Electromagnetic Instruments, Inc.

ABSTRACT

A collaborative effort has been undertaken between Lawrence Berkeley National Laboratory, Sandia National Laboratories, The Hawaiian Volcano Observatory of the U.S. Geological Survey, and Electromagnetic Instruments, Inc. to study Kilauea Volcano, Hawai`i using the magnetotelluric (MT) technique. We present results from the first phase of data aquisition, recorded in August 2002, where 33 MT sites over the summit region as well as the southwest and east rift zones were acquired. Good-to-excellent-quality data were obtained, even under the harshest conditions, such as those encountered on fresh lava flows of the east rift zone, where electrical contact resistances are extremely high. Electrical conductivity anomalies resulting from two-dimensional inversion of sites, sorted into profiles, had a high degree of spatial correlation with previously published seismic velocity anomalies observed beneath Kilauea Caldera. In particular, we have been able to map regions of active magma transport and storage beneath the locus of current east rift zone activity near the Pu`u O`o-Kupaianaha vents, and in adjacent areas. In addition, we have resolved upper portions of the vertical magma ascent conduit beneath the summit caldera. Low-resistivity domains of magma storage beneath Halemaumau and the southwestern caldera region have also been resolved. Active fault zones imaged by seismic velocity tomography as low velocity zones tie to low resistivity zones beneath the inverted MT lines. Groundwater-saturated regions within the Kaoiki fault zone have been resolved in 2-D cross-sections. In the Hilina fault zone, we have resolved regions of inferred saline waters, forming conductive domains within these fractures over the depth range 1 to >6 km. We have also undertaken a three-dimensional (3-D) MT model study of Kilauea Volcano,

portions of the island of Hawai`i, and the surrounding ocean, to better access the roles these features play in the observed MT measurements. Results of the 3-D model studies lend confidence to the data sensitivity of the magmatic structures beneath the volcano, and our ability to properly model island topography and coastal effects.

INTRODUCTION

The electrical conductivity of rocks, minerals, and fluids is one of the most temperature- and composition-sensitive measures of the transport properties of earth materials. Measurements of the *in situ* electrical impedance of domains within active volcanoes–conducted over a broad frequency range–guarantees that we will be dealing with a wide range of phases, compositions, and compositional gradients distributed quite heterogeneously over a great span of temperatures, and pressures. For active Hawaiian volcanoes, we anticipate complexities in the arrangements of their electrically conductive magmatic passageways, in their interconnected hydrothermal conduits, and in their shallow groundwater-bearing porosity. Part of this anticipation is based on our understanding of earth materials and active transport pathways directly observable in the near surface, and partly on the study of related fossil pathways (e.g., dike swarms and vein networks) in the eroded interiors of the ancient and extinct volcanoes elsewhere in the Hawaiian chain. For Kilauea (Figure 1), *in situ* resolutions of such electrically conductive pathways and domains at kilometer (and greater) scales offer the possibility of providing additional new information on how magma and hydrothermal fluids are stored and migrate at depth.

Previous electrical and electromagnetic (EM) investigations of Kilauea have focused on techniques that make use of a controlled source of electrical (DC resistivity) or electromagnetic (frequency and time-domain EM sounding) energy. While previous studies have provided useful information about Kilauea's electrical structure, they have suffered from two primary limitations. First, the depth of penetration has been limited by practical limits on the power available to man-made transmitters. Second, at the time of previous controlled-source experiments, the 3-D computer modeling of electromagnetic data was in its infancy, thus limiting interpretations to one-dimensional (1-D) models. In recent years, the second limitation of controlled source methods has largely disappeared, while the first limitation is still present.

The magnetotelluric (MT) method overcomes the issues of depth penetration by using the natural EM radiation that bathes the earth as a power source, in conjunction with the use of suitably low frequencies during measurement. Thorough explanations of the MT method in general, and its use in exploration in particular, are given in Vozoff (1996) and in Orange et al. (1989), respectively. MT has been used extensively in volcanic and geothermal investigations world-wide (Park et al., 1988; Nolasco et al., 1998; Ogawa et al., 1999; Matsushima et al., 2001). However, previous attempts at using MT at Kilauea have been disappointing and have not been reported in the literature. In this paper, and in the companion Part I paper by Gasperikova et al. (2003), we report the first successful MT experiment on Kilauea.

The objectives of the project that acquired the data set reported here are broader than the scope of either the Part I or Part II papers. The overall project objectives are: (1): to produce a high-quality MT data set over the summit caldera and the east rift zone and southwest rift zone, a

data set that is capable of supporting 3-D inversion for conductivity structure; (2) to use this data set to drive the continued development of new 3-D MT inversion algorithms; and (3) to integrate existing geologic, gravity, seismic, deformation, electrical, and physical property data with the new MT measurements to provide a new understanding of the internal structure of the volcano. In this paper, we report on the two-dimensional (2-D) inversion of the data collected in August 2002 and compare the derived 2-D images of the resistivity structure to previously published studies of the seismic velocity structure. In addition, we present results from a 3-D MT model study of the volcano, the island of Hawai`i, and the surrounding ocean, to better understand the 3-D effects in the data. Thus, the study represents a first step towards a full 3-D inversion of the field data.

MAGNETOTELLURIC DATA AND DATA PROCESSING TECHNIQUE

The MT data for this survey consist of measurements of horizontal orthogonal electric (E) and magnetic (H) fields that are related to each other through the electromagnetic impedance tensor (Z):

$$\begin{bmatrix} E_x \\ E_y \end{bmatrix} = \begin{bmatrix} Z_{xx} & Z_{xy} \\ Z_{yx} & Z_{yy} \end{bmatrix} \begin{bmatrix} H_x \\ H_y \end{bmatrix} \quad (1)$$

Good data quality was achieved over the frequency range 0.0002 to 100 Hz. A set of nine prototype MT systems provided by Electromagnetic Instruments, Inc. were used with a deployment schedule that attempted to have at least five MT systems recording at any given

time. This allowed the use of recently developed robust MT processing algorithms (Egbert, 1997) that simultaneously process all input MT channels. These algorithms have been demonstrated to produce superior data quality when compared with conventional remote reference (Gamble et al., 1979) MT data processing techniques. Details of the MT data processing procedure are described in the companion paper by Gasperikova et al. (2003). As Part I describes, several factors affect data quality, including total recording time, the number of magnetic channels available at other sites, and the local EM noise. Figure 2 illustrates the off-diagonal (Z_{xy} and Z_{yx}) apparent resistivity and phase curves as a function of frequency at the Keller-NSF site and at site S05, (Figure 1). The Keller-NSF site represents the best data quality obtained by recording for a 72-hour period, whereas site S05 represents a more typical 48-hour recording.

The ultimate goal of the project is to use a fully 3-D algorithm (Newman and Alumbaugh, 2000; Newman et al., 2002) to invert the MT data and produce a 3-D conductivity model of the interior of Kilauea and its rift zones. However, data collection will not be complete until the end of 2003. As an initial stage in evaluating the data acquired to date, we have constructed linear profiles of sites from the first data collection phase and inverted these profiles using 2-D inversion. For the inversion, we employed the nonlinear conjugate gradient 2-D algorithm of Rodi and Mackie (2001). Figure 3 illustrates the site distribution, together with the surface elevation and the six site transects (Lines 1 through 6) that were inverted for the 2-D resistivity structures. The outline of the magmatic internal structure is from Ryan (1988; Figure 19 of that report), projected upwards to a depth of 1 km. In areal extent, it includes regions of known eruptive vents, fracture swarms within the rift zones, gravitational collapse features

(craters), geothermal vents, and centers of uplift related to inferred dike formation events as constrained by finite element and analytic continuum models of rift zone deformation–all projected in planform to the near-surface.

ON THE 3-D DISTRIBUTION OF ROCK, MELT, MAGMA, AND AQUEOUS FLUIDS: THEIR PROPERTIES IN RELATION TO BULK MAGNETOTELLURIC AND ACOUSTIC PARAMETERS

Hawaiian volcanoes are built from a succession of relatively thin lava flows spanning a thickness range from roughly 1 to over 6 m (Easton, 1987; Holcomb, 1987; Lockwood and Lipman, 1987). Within-flow structural variations at shallow depths are hydrodynamically important, and subhorizontal permeabilities along differentially porous lava flow bases are frequently several times their vertical equivalents (Takasaki, 1978; Thomas, 1987). Because of their high permeabilities, lava flows may be considered fully saturated below the water table, or only partially wetted above the water table. Previous surface and borehole studies (Zhody and Jackson, 1969; Zablocki et al., 1974; Jackson et al., 1985) have shown the saturation to be a sharp transition at the water table. At great depth, metamorphism from greenschist to amphibolite facies alters primary mineralogies and obliterates primary textures through replacement reactions and void-filling mineralization. Lacing these basalt successions together vertically and horizontally are swarms of subsolidus and still-molten intrusions within and beneath the active rift zones, ascent pathways, and magma storage centers (Ryan et al., 1983; Walker, 1987). In physical scope, our field measurements have sampled Kilauea to the 8–10 km

depth level, and encompassed an areal extent that measures 20 km by 40 km. Thus the total volume sampled extends from the flanks of Mauna Loa to the Hilina Pali, and from Kilauea's summit to the base of the volcanic shield. Physiographically, this includes the summit caldera and major portions of the southwest and east rift zones. The included volume is approximately 8,000 km^3.

Interpreting electrical resistivity images produced by the inversion of MT data in terms of geologic structure and process requires an understanding of those factors governing the electrical conductivity of earth materials. An inventory of the electrical conductivties of Hawaiian rocks, minerals, melts and aqueous fluids reveals that all are sensitive to changes in composition, material anisotropy, defect solid-state, porosity, temperature, and pressure (Tyburczy and Waff, 1983, 1985; Tyburczy and Fisler, 1995; Rai and Manghnani, 1977, 1978, 1981; Llera et al.,1990; Olhoeft, 1977; Quist and Marshall, 1968; Frantz and Marshall, 1982; Frantz et al., 1993; Ucock et al., 1980). *In situ* electrical resistivities as determined by inversions of field measurements are *bulk* properties and sample the integrated response of large heterogeneously-arranged volumes. With respect to Kilauea, such volumes may contain mixtures of two or more solids, single phase melts, multiphase melts (magma), aqueous fluids, and/or gases. The integrated electrical response is thus a measure of summed individual "single component" contributions, in some volume-averaged sense. Our inversions of field data have suggested resistivity values that span about five orders of magnitude, from highly resistive new lava flows at $Log_{10} = 4$ [10,000 Ω-m], to highly conducting melt approaching $Log_{10} = -1$ [0.10 Ω-m]. Embeded within this range are the individual contributions of the pure and mixed phases and their pressure-temperature responses, as discussed above.

Interpretive challenges include dealing with the range of electrical resistivities for solid and liquid compositions relevant to Kilauea that show significant *overlap*. Such overlapping resistivity ranges may frustrate, in principle, attempts to uniquely isolate the material contributor(s) to a given *in situ* resistivity value. "Resisitivity overlap" is particularly notable with respect to magmas and saline pore fluids in which (for example) crystal-free magma with resistivity values spanning 1.8 to 0.2 Ω-m (Rai and Manghnani, 1977; Tyburczy and Waff, 1983) may completely bracket the sea water resistivity in adjacent fractures [0.33 Ω-m; Hermance (1995)]. Well-constrained acoustical data (Ryan, 1987a) suggests that Hawaiian volcanoes are aqueous-fluid permeable to depths of 9–10 km, and are capable of maintaining intermittent hydrostatic fluid connections from those depths to the surface. Identical depth estimates have been independently corroborated for equivalent lithologies elsewhere (Hermance, 1973). Shallow (i.e., 500 m to 2 km) hydrothermal systems will continuously exploit this permeability depth dependence, and the upper sections of magma reservoirs, dike swarms, and rift zone magma storage regions are expected to be mantled, ubiquitously, by aqueous pore fluids at hydrothermal temperatures.

Thus, for several of the closed-contour resistivity lows in the inversions of this report, we are looking at magma storage regions through the veil of a surrounding hydrothermal shroud. Should those surrounding pore fluids evolve towards brines (Fournier, 1987), the potential for "resistivity overlap" may well increase and lead to yet added complexities in the MT data interpretation (Ucock et al., 1980). The effect of porosity, pore water salinity, and temperature on the bulk resistivity of tholeiitic basalt is summarized in Figure 4 (Kauahikaua et al., 1986).

For low temperatures (below 600°C) two cases are considered: (a) for low salinity pore water (groundwater from the Keller-NSF research drill hole [Kauahikaua, 1982]) and (b) for sea water. Above 600°C, conduction through the rock matrix exceeds conduction through the pore electrolite, and the resistivity decreases with increasing temperature. In sum, zones of relatively crystal-free and bubble-free magma within Kilauea should exhibit resistivity values of less than 2 Ω-m, compared with nonmagmatic regions (at requisitely high volume fractions of fluid). Well-developed fault zones should also exhibit lower resistivity and seismic velocity due to fracturing and increased water content, if the fluids are suitably brackish. Fluid salinities will of course progressively increase as the proximity to the coast increases. The survey of Flanigan and Long (1987) resolved narrow and fan-like low-resistivity sections within the volcanic flanks which correlate spatially with some 40-45°C springs near the coastline and have source regions that are considerably higher within the volcanic flanks. The salinities of the relevant groundwater beneath these fan-like zones is currently unknown, as are their 3-D connections to the interior of the volcano.

Like electrical conductivity, the seismic velocity of rock is also a function of porosity and fluid saturation. Fractures and included melt both have the effect of decreasing compressional and shear wave velocities and elastic moduli, and increasing Poisson's ratio (Budiansky and O'Connell, 1976; Berryman, 1995; Mavko, Dvorkin and Nur, 1998). Limited experimental data on the effects of small melt fractions exists for peridotite at 5 kbar (500 MPa) confining pressure (Murase and Kushiro, 1978) and show decreases of about 5 % in V_p after the production of approximately 7–9 % melt. In these experiments, the melt phase was distributed along grain boundaries and triple junctions, until a 27% melt fraction was achieved, at which time all grain

boundaries were wetted. Overall, the measurements showed a relatively slow rate of falloff in V_p with increases in melting, until 18 melt % at which time then velocity falloff accelerated. The calculations of Mavko (1980) and Takei (1998), on the other hand, indicate that 1% melt fraction induces V_p to decrease between 10 and 40%, whereas V_S correspondingly decreases between 20 and 100%. Theoretical evaluations, however, depend critically on the geometric distribution(s) of the melt phase, with low-aspect-ratio inclusions producing the greatest velocity decrease, and equant (spherical) inclusions producing the least (Walsh 1969; Ryan, 1980). In addition, Murase and McBirney (1973) have measured the 1 atm compressibility of basalt over the melting interval, inverted for the bulk modulus, **K**, and found changes from **K** = 7.5 x 10^{11} dynes cm^{-2} to 1.5 x 10^{11} dynes cm^{-2} over the entire melting range. In general, highly fractured magma-bearing regions will have the highest V_p/V_S ratio, relative to intact rock with no resident magma. Fracture zones within the shallow portions of Kilauea induce low *in situ* V_p (Ryan, 1987a, pp. 1423–1434). At shallow depths and low confining pressures, high porosities correlate with low V_p and bulk frame moduli for basalt, however high V_p/V_S ratios require the differentially low shear wave velocities that are associated with high magma fractions and/or or high volume fractions of aqueous pore fluids at higher than hydrostatic pressures. Such regions of high magma fraction will correlate with low V_p and elevated V_p/V_S .

Our philosophy of data interpretation involves using multiple working constraints, and this has been employed in several ways. In some instances, magmatic and hydrothermal resistivity signatures may be physically separated in our interpretations of the inverted MT resistivity sections, because saline aqueous intrusions and the heat sources that drive their migration are separated in depth. In other instances, prior relatively high-resolution seismic

tomography experiments have yielded maps of compressional wave velocity and/or V_P/V_S values, maps that may be compared side-by-side with MT resistivity values for the same domain within the volcanic interior. In still other comparisons, well-constrained subsidence deformation analyses have illustrated the geometry of geologic structures responsible for magma storage within our domains of low resistivity. In sum, we have avoided using a solitary approach, wherein the results of our magnetotelluric study would otherwise be interpreted in isolation from other relevant work.

SPATIAL VARIATIONS IN MAGNETOTELLURIC FIELDS

A very useful representation of the MT impedance tensor is the "polar plot". In this plot, the magnitude of the off-diagonal and on-diagonal elements of the impedance tensor (Equation 1), at a selected frequency, are calculated as the coordinate system is rotated through 360 degrees. Because the off-diagonal impedance is the ratio of orthogonal E and H fields, an off-diagonal polar plot will have the appearance of a peanut oriented in the direction of large E fields or perpendicular to the direction of small H fields. The on-diagonal terms of the impedance tensor represent the ratio E/H in parallel directions. This property can be used to locate vertical or near-vertical contacts between resistive and conductive material by looking at the spatial distribution of the polar plots. In particular, for a line of sites traversing across a geologic contact between resistive and conductive rock, the off-diagonal polar diagram “peanut” will point toward the contact on the resistive side and be oriented parallel to the contact on the

conductive side (Vozoff, 1996). These orientational effects are caused by the large electric fields in the resistor that sharply drop across the contact with the conductor.

Polar diagrams permit a quick inspection of the orientation of the E and H fields, as well as the dimensionality of the data. Over a one-dimensional isotropic earth, the magnitude of the off-diagonal terms plot as a circle (E and H fields are independent of orientation) with the on-diagonal terms equal to zero (no cross-coupling occurs between E and H). Over a two-dimensional earth, the off-diagonal curve forms a peanut shape, and the on-diagonal curve forms a symmetric four-leaf clover (much smaller than the off-diagonal terms). Over a three-dimensional earth where non-orthogonal E and H can be coupled, the on-diagonal terms become asymmetric and can be as large or larger than, the off-diagonal terms.

The impedance polar diagrams constructed at 0.01 Hz are illustrated in the survey transect configuration map of Figure 3 at selected measurement sites. The magnitude of the off-diagonal terms is in black; the magnitude of the on-diagonal terms is in red. The 0.01 Hz data are representative of the low-frequency data up to nearly 1 Hz. Above 1 Hz, less dimensionality is seen in the data, with polar diagrams becoming more one-dimensional in nature. Figure 3 shows that the average electric field strike is oriented N45°W in the western portion of the survey, whereas the E-field strikes roughly N10°W in the eastern sector. The spatial orientations of the maxima of the off-diagonal terms align perpendicular to the strike of the rift systems. Line 1 lies roughly along the strike of the E-field, so that Z_{xy} and Z_{yx} are oriented parallel and perpendicular to the "electric strike", thus allowing both to be modeled in the 2-D inversion as TM and TE, respectively. Data for the other five lines (which were neither parallel nor

perpendicular to the electric strike) were rotated so that E is in the line direction and H is perpendicular to the line direction. With this rotation, the Z_{XY} impedances are considered to be the TM mode for the 2-D inversion. Thus, the inversion for Line 1 was a joint TE, while TM inversions and the remaining lines used TM (Z_{XY}) only.

THREE-DIMENSIONAL NUMERICAL MODELING

Because this MT survey has been conducted on an island with varied and rough topography, the effects of the surrounding Pacific Ocean as well as the topography must be considered in any modeling of the data. Ocean effects are caused by long-period electric currents, induced in the conductive ocean, that collide with the resistive land, causing them to abruptly change direction as they flow around the island. The distortion of current caused by the island produces distortions in the measured MT response on the island (Mackie et al., 1988). To access the magnitude of these "island effects", we have constructed a 3-D numerical model of the entire island of Hawai`i, complete with the surrounding bathymetry out to several hundred kilometers. The land was modeled as a 100 Ω-m material surrounded by 0.333 Ω-m sea water. The response was calculated between 100 and 0.0002 Hz. This 3-D response was compared to the 2-D response for cross-sections through the island that were coincident with the six data profiles (lines) of Figure 3. At the data collection sites, it was found that the topography and the effects of the surrounding ocean caused the 3-D response to differ from the 2-D response below 0.01 Hz (usable data extends to 0.0005 Hz). These results are consistent with similar coastal effect calculations conducted by Santos et al. (2001). Based on our 3-D calculations, we limited

the frequency to greater than 0.01 Hz for the 2-D inverse models presented here. Kilauea's topography along the profiles, as well as the effect of the Pacific Ocean, is modeled in the 2-D inversions.

The 3-D model used for assessing the topography and coastal effects discussed earlier was modified to add the 3-D magmatic internal structure presented by Ryan (1988). The model incorporates the upper level of intrusion, dike formation, and faulting at 1 km depth, with subrift zone and subcaldera magma storage regions projected vertically downward to 10 km depth, the base of the volcanic shield. Beneath the 10 km depth level, we constructed a magma conduit through the oceanic crust and into the upper mantle to a depth of 40 km, based on Ryan (1988). The magmatic conduit and the magma-charged rift zone cores were assigned a resistivity of 1 Ω-m embedded within a 100 Ω-m country rock host. The model had 107 × 103 × 123 cells in the x, y, and z-directions, respectively. Cells in the area of the survey (the southeast (Kilauea) quadrant of the island) were 1,000 × 1,000 × 200 m in the x, y and z-directions, respectively. Cell dimensions graded to progressively larger sizes towards the boundaries of the model, reflecting decreases in required spatial resolution. Figure 5 illustrates a plan view of the central portion of the mesh at sea level. Frequencies from 0.0002 to 100 Hz were calculated with a parallel forward modeling code (Newman et al., 2002), using 125 processors.

The polar impedance diagrams from the 3-D model at 0.01 Hz are displayed in map view in Figure 6 for comparison with Figure 3. Field data shown in Figure 3 illustrate that within the western portion of the study area, the impedance maximum is oriented approximately N45°W, and is roughly perpendicular to the strike of the southwest rift zone (SWRZ). In the eastern

portion of the volcano, the impedance maximum is oriented roughly north-south, or approximately perpendicular to the east rift zone (ERZ). Although the deep-shield magma reservoir discovered by Ryan (1988) dwarfs the classical subcaldera "summit" reservoir in both volume and maximum dimensions, the Keller-NSF site is *somewhat* unique in that it is located over the center of the largest *relatively shallow* conductive mass within the caldera region–that is, the summit magma reservoir. Here, the impedance maximum in the field data is oriented east-west. Site S09, situated near the southern margins of Kilauea Caldera and above the south-dipping conduit (Ryan, 1988) has its maximum impedance orientation located between that of site J44 and the Keller-NSF site, indicating a transition region from resistor to conductor.

In general, the modeled data for spatial variation in the orientation of the polar diagrams agree well with field measurements. To the west, both the field-determined and the model impedance polar diagrams are generally oriented perpendicular to the SWRZ, while in the east, they are oriented perpendicular to the ERZ. At the Keller-NSF site and at site S09, the 3-D model results show fewer changes in the shape of the impedance polar diagrams. The model "polars" at the Keller-NSF site and site S09 change from strongly 2-D to the northwest to nearly 1-D (~ isotropic) at the Keller-NSF site, with slightly less of a 2-D to 1-D transition at site S09. This implies that the model magmatic structure is either not large enough, or does not have a low enough resistivity. However, the *nature* of the change is generally consistent with the field data. To the east, at sites J21 and J23, the model and the field data agree quite well. This comparison lends confidence to both the data sensitivity-to-magmatic-structure and our ability to model (and in the future, invert) in 3-D.

LIMITATIONS IMPOSED BY TWO-DIMENSIONAL MODELING

In two-dimensional inversion, the depth of investigation is limited by the 0.01 Hz cut off in the frequencies used for the inversions. This frequency limit, in combination with a regularized (smooth) inversion with a 100 Ω-m half-space starting model, produces a specific type of artifact in the inverse models. All features (conductive or resistive) that differ from the starting model fade back to starting-model values at depths where significant response occurs below the 0.01 Hz cutoff frequency. The depth from which no information is present in the data above 0.01 Hz depends on the integrated conductance above, which varies over the survey area. In general, the depth sensitivity cutoff in areas with substantial regions of low resistivity is between 6 and 10 km. Resistive areas have a larger depth of investigation. Therefore, termination of conductive features with depth, below 6 to 10 km, does not necessarily mean that the (low resistivity) structure terminates. In the context of the Kilauea Volcano, we know that the deep cores of both the southwest and east rift zones contain an upper gabbroic and lower picritic melt+olivine+pyroxene-dominated crystal mush over the 5 to 10 km depth interval (Ryan, 1988, pp. 4244–4246). This crystal mush should be relatively conductive on top and increasingly resistive with depth, based on the end-member conductivities (melt, olivine, pyroxenes, spinel, and plagioclase) and simple mixing-model considerations for compacting two-phase mixtures. In addition, the primary conduit extends to at least 35 km depth with considerable spatial and temporal coherence, based on comprehensive microseismic surveys (Ryan, 1988; Klein et al., 1987).

One impact of limiting the frequencies utilized to greater than 0.01 Hz is that one can only resolve the tops of some of the most interesting features, such as the magma conduit to the mantle (as proposed by Ryan (1988)). The entire resistivity structure beneath Kilauea and its rift systems will be extended in depth by full 3-D inversion of the complete data set after the 2003 data aquisition. At that time, and with a depth sensitivity to at least 20 km, we will also be able to compare our resistivity models to density models produced by Kauahikaua et al. (2000). The density contrast surface presented there falls, in general, just below the depths where the 0.01 Hz-limited MT data are sensitive. In addition, resolving the 3-D resistivity of Kilauea to depths significantly beneath the 10 km permeability limit for aqueous fluids will effectively separate the shallow contributions of saline pore fluids, from the deeper signatures of melts and rock matrix only.

TWO-DIMENSIONAL MAGNETOTELLURIC INVERSIONS

Figure 7 illustrates the 2-D inversion for Line 1 (see Figures 3 and 6) with the observed and calculated TM mode apparent resistivity and phase shown in Figure 8. The data was averaged to five points per decade prior to inversion. The general resistivity structure to the north of the caldera is quite similar to that found by Kauahikaua et al. (1986, Figure 14), with near-surface high resistivity rocks becoming more conductive near 2 km depth. The shallow transition from high to low resistivity is most likely associated with the water table. At the Keller-NSF site, a research hole drilled in 1973 resolved a sharp resistivity gradient (high to low) then associated with the base of the unsaturated zone (Zablocki et al., 1974). The water table is

at a depth of about 500 m below the surface, corresponding to the sharp high-to-low gradient in resistivity in the inverse model at that location. The conductive zones beneath sites S02 and S03-S04 correspond to the location of the Kaoiki fault zone (Okubo et al. 1997). (The correlation between seismic velocity tomography and this resistivity image will be considered further, below.) The 2-D MT resistivity image for Line 1 and the cross-section constructed from 1-D inversion (Kauahikaua et al. 1986, Figure 14) do not match south of the caldera. In this general portion of the volcano, the subcaldera magma reservoir merges with the southwest rift zone and the Halemaumau connections with the east rift zone, both of which intersect at an acute angle enclosing the Koae fault zone between. In addition, the SWRZ and the ERZ are continuously cored by an ultrabasic deep-shield magma reservoir (Ryan, 1988) that passes continuously through the roots of the summit reservoir. Supplying all of this, and providing the fluid linkage to the upper mantle, is the primary magma conduit. Thus, all of these magma transport and storage structures collectively comprise a 3-D region from an electrical resistivity perspective. In such a setting, we would expect 2-D inversion to be more accurate than 1-D inversion, although both are, of course, only approximations.

The conductive anomalies between site S08 and the Keller-NSF site, as well as between the Keller-NSF site and site S09 on the Line 1 2-D inverse (Figure 7), are located within the boundaries of the summit magma reservoir mapped by Ryan (1988). Station S08 lies just to the north-northwest of Halemaumau, whereas station "Keller-NSF" lies west-southwest of Halemaumau. The deeper somewhat south-dipping conductor beneath site S09 is in the correct location for the magma conduit from the mantle. As noted earlier, the termination of the low resistivity structure interpreted as the primary magma conduit to the mantle south of Line 1 can

be produced by "regularization smoothing" the model back to the starting values. The magma conduit has expressions on other 2-D lines, as we will see below in the fence diagrams viewed in 3-D perspective. Finally, the remaining five major survey lines have been inverted to recover their 2-D electrical resistivity cross-sections at depth. Each of these five sections (plus Line 1) form the primary distance-depth slices through Kilauea that comprise the fence diagrams viewed in 3-D perspectives below.

ASSEMBLED TWO-DIMENSIONAL MAGNETOTELLURIC INVERSIONS IN THREE-DIMENSIONAL PERSPECTIVES AND THEIR CORRELATIONS WITH SEISMIC TOMOGRAPHY

Figure 9 illustrates the 2-D resistivity images for MT Lines 1 and 6, and presents several features of interest. The Line 6 section beneath the Pu'u O'o-Kupaianaha vents shows a closed-contour low-resistivity region (< 17 Ω-m) in the 3–5 km depth interval. This is roughly 2 to 4 km below sea level (b.s.l.), and corresponds closely to the region of neutral buoyancy for tholeiitic magma (Ryan, 1987a,b). We associate this relatively conductive domain with the local magma storage *region* for the Pu'u O'o-Episode 54-Kupaianaha eruption series. The residual melt lens in the 1959 Kilauea-Iki lava lake had a resistivity of about 10 Ω-m (Anderson, 1987) by the late 1970's and early 1980's. Because the bulk resistivity resolved in this section is somewhat above the expectations for melt alone (most conservatively, 1.75 to 0.10 Ω-m), we infer that the conductive volume contains subsolidus country rock as well as magma. We note also that systematic studies of the aggregate electrical conductivity of melt+crystal+bubble

mixtures to mimic the response of magmas have yet to be conducted, either theoretically or experimentally, but second-phase particles would be expected to *lower* the *bulk* conductivity values. Line 1 contains low-resistivity domains below the surface expression of the Kaoiki fault zone, and these are in the 1 to 2 km b.s.l. depth range. The combination of low resistivities (10 to 5.6 Ω-m) and their location within the Kaoiki fault zone, and well to the north of documented regions of magma storage and migration, suggests somewhat brackish pore fluids in a moderately altered basalt matrix. Indeed, these resistivity values correspond to those found in the lower portions of the Keller-NSF drill hole (Zablocki et al., 1974).

The electrical resistivity structure resolved by MT may also be correlated and intercompared with seismic velocity anomalies imaged by prior studies. Dawson et al. (1999) used seismic tomographic inversion of both P- and S-wave arrival times from local earthquakes to generate P- and S-wave velocity images beneath Kilauea Caldera. Our MT inversions may now be compared with the V_p/V_S ratio from Dawson et al. (1999, Figure 3b). The color scales for resistivity and V_p/V_S ratio have a different color "polarity". Reds in the resistivity image indicate low resistivity, whereas red in the Dawson et al. (1999) report indicate high V_p/V_S. For both scales, however, reds correlate *materially* with relatively dilatent fluid-charged rocks– capable of differentially conducting electric currents, but incapable of efficiently transmitting shear waves.

The low-resistivity (red) region on Line 1 between site S08 and the Keller-NSF site lies beneath the western portion of Halemaumau and the connection between Kilauea Caldera and the upper southwest rift zone (Figure 9). It is spatially coincident with the shallow western

sections of the summit reservoir mapped by Ryan et al. (1981), and corresponds to the uppermost reaches of sill-like magma storage compartments, as demonstrated by Ryan et al. (1983) for caldera-wide subsidence analyses. This region has a closed-contour low resistivity core that is appreciably below 5.6 Ω-m and is consistent with a magma-impregnated zone of slightly brackish hydrothermal fluids. The region also correlates spatially with the anomalously high V_P/V_S ratio (red) found beneath the southwest section of the caldera (Dawson et al., 1999). The high V_P/V_S ratio and the associated high Poisson's ratio of 0.32 suggest the presence of either heavily fractured rock–fully or partially saturated with aqueous fluids–and/or a significant fraction of magma. The resistivity on Line 1 in the correlation region, with the V_P/V_S anomaly of Dawson et al. (1999), reaches a low of 3 Ω-m. Based on the resistivity-temperature relationships of Rai and Manghnani (1977), Manghnani and Rai (1978), Tyburczy and Waff (1983), and the summary of Kauahikaua et al. (1986), this resistivity correlates with a temperature of about 1250°C, supporting the interpretation of a significant volume fraction of magma beneath the southern portion of the caldera. In addition, Saccorotti et al. (2001), Ominato et al. (1998), and Almendros et al. (2001) have drawn attention to the substructure of Halemaumau and its role in shepherding magma batches into the upper east rift zone (in addition to shallower hydrothermal effects).

The southern portions of the shallow subcaldera magma reservoir is imaged on MT Lines 1, 3, and 6. Nevertheless, the conductive region, centered at a depth of 2.5 km beneath the surface on Line 6 (near the caldera) plunges to the south on Line 1 and is intersected by Line 3, where the center of the conductive region is at a depth of 5.2 km below the surface. Shallower, sub-Halemaumau sections of the uppermost reaches of the reservoir are shown on Line 1, as

remarked above. Despite the resolution of portions of the subcaldera magma reservoir, however, there remains some miss-tie in resistivity values at the Line 1-3-6 intersections.

In Figure 10, Lines 1,3,4,5, and 6 are assembled in a north-northeastward-looking perspective. In the figure, relatively shallow resistivity lows associated with hydrothermal fluids are seen, as well as deeper regions of stored magma beneath both the summit region and the east rift zone. All form closed-contour resistivity lows. Along the visable portions of Lines 1 and 5, shallow hydrothermal fluids migrating southward along the buried slopes of Mauna Loa (6–17 Ω-m) traverse first through the Kaoiki fault zone and then navagate the dike complex of the upper southwest rift zone, traveling down a regional hydraulic gradient in the process. At the western end of Line 3, resistivity lows of 6–17 Ω-m core a region between 2 and 6 km b.s.l. (about 3 to 7 km below the surface), and this is generally coincident with the tholeiitic horizon of neutral buoyancy for Kilauea (Ryan, 1987a, b) and its juncture with the deep-shield, ultramafic magma reservoir. In plan form, it occurs below the bend in the east rift zone and lies somewhat west of Mauna Ulu. We interpret this region to be dominated by subrift magma storage, with contributions from adjacent hydrothermal fluids. Finally, the magma storage region beneath the Pu'u O'o-Kupaianaha vents is seen again on the depth expression of Line 6.

Haslinger et al. (2001, Figure 4) present V_p tomograms on two lines that are roughly orthogonal to the east rift zone and lie east of Mauna Ulu. These have been added to Figure 10, where they are denoted as profiles A-A' and B-B'. On these two profiles, the high seismic velocities correlate spatially with the high resistivities of our MT survey, particularly in the 6–8 km depth levels. These high subrift resistivities (100–300$^+$ Ω-m) and high seismic velocities (~8

km s^{-1}), taken in combination with their particular depth levels, invites an association with olivine-rich cumulates that have been suggested to core the lower levels of the east rift zone (Ryan, 1988; Clague et al., 1995). This high-resistivity region continues to the east along MT Line 3 with its intersection with Line 6. At this intersection (just west of the Hasling et al. profile A-A'), there is a slight miss-tie in the resistivity values, although the structure there is inferred to be laterally continuous. At greater depths, the gradation from low to high resistivity at depths of 8 to 10 km will be caused by the regularization process smoothing the model back to the starting values (100 Ω-m), due to limited depth sensitivity in the band-limited data.

Seaward of the east rift zone (Figure 10), along profiles A-A' and B-B', are deep domains of anomalously low compressional wave velocity. These domains are much too far to the south to be associated with magma, but they do have a very high spatial correlation with the high b-value domains of Wyss et al. (2001). In their study, Wyss et al. (2001) mapped domains at intermediate and large depths within the south flank that are characterized by relatively large numbers of small earthquakes–thus shifting the earthquake magnitude coefficient (the b-value), to high numerical values. These domains are, in turn, congruent with several of the south flank tectonic blocks illustrated in Ryan (1988, pp. 4235–4242), and they are inferred to be relatively dilatant and charged with high pore-pressure aqueous fluids.

From a southeastward-looking perspective above the flanks of Mauna Loa (Figure 11), Kilauea's electrical resistivity structure is illustrated by combining all six inverted survey lines. This view highlights the resistivity low of the magma storage region beneath the Pu'u O'o-Kupaianaha vents (beneath the eastern portion of Line 3). In addition, and appearing as a thin,

near-surface orange-red veneer beneath Lines 5 and 6, are the very shallow resistivity lows inferred to be hydrothermal circulation zones in altered basalt sequences. Note that Lines 3 and 6 are essentially "piecewise-parallel" to what is a continuously changing planform azimuth of the east rift zone itself. The straight and rectilinear panels of the survey traverses are, in turn, crossed over (penetrated) by the complex rift zone structures themselves at depth, suggesting (for example) apparent breaks in lateral magma continuity. We believe that these resistivity continuity breaks are more apparent than real. Of course, filling in these gaps will require additional rift zone crossing lines, as well as overall increases in the density of along-line station coverage. Suffice to say that the internal structure of the east rift zone is not geometrically regular in either cross-section or in plan form, but is fully three-dimensional on all scales.

In the right-central portion of Figure 11, MT survey Line 2 lies above two remarkable lobes of low resistivity. Spatially, one of the lobes is located within the area of the Hilina fault system, and the other one lies slightly to the north of the Hilina. Located within the volcanic flanks, they are much too far removed to the south of the rift zones and caldera to be *directly* associated with magma. The most southwesterly of these lobes lies approximately within the plane of the Hilina faults themselves. The northeasterly lobe, however, lies roughly orthogonal to the apparent Hilina fault trend, and is instead crudely parallel to the strike of the upper east rift zone, but removed 4–5 km to the west. The resistivity lows lie beneath sites S24 and S22, but considerably south and southwest of the geothermal areas of the upper east rift zone (e.g., Bartel and Jacobson, 1987). The resistivity in the core of the southwesterly lobe is < 1.77 Ω-m, while the resistivity in the northeasterly lobe is on the order of 1 Ω-m, or less. The depth of the southwesterly lobe ranges from 1 to about 3 km, whereas the depth of the northeasterly lobe is 1

to as much as 6–7 km. We note that the resistivity of sea water is 0.33 Ω-m, and that moderate dilutions with shallow nonsaline waters would produce the requisite resistivities in the range 1.75-1.0 Ω-m. We suggest that sea water has gained access to the roots of the Hilina fault system, and–after being heated by deep south flank rocks–is advected upwards to mix with higher-level meteoric water flowing southward at shallow-to-moderate depths, just south of Kilauea Caldera.

Figure 12 (view from the southwest) illustrates the duality of the inferred less-conductive hydrothermal fluids flowing down the buried flanks of Mauna Loa within the Kaoiki fault zone, and the inferred relatively saline hydrothermal fluids rising within the Hilina fault zone. In the Kaoiki, domains of low resistivity (10 to 5.6 Ω-m) resolved by inversions of Line 1 show as medium yellow-to-light orange [1.0 to 0.75 Log_{10} resistivity units]. In the Hilina fault zone, the hydrothermal lobes that we believe to be relatively saline show up as deep orange-to-orange-red [0.25 to 0.0 Log_{10} resistivity units] in inversions of the Line 2 stations. This figure also includes the 1–3 km depth slice from the tomographic study of Okubo et al. (1997), where low V_p values in the Kaoiki fault zone correlate spatially with the low resistivities of the MT inversions. In addition, the Okubo et al. (1997) results show an additional low velocity region due south of the east rift zone (V_p about 4.0 to 4.5 km s^{-1}). These low velocities are not related to magma, but *are* spatially correlated to the upper portions of the domains of high b-values mapped by Wyss et al. (2001). We interpret these domains, identified by both Wyss et al. (2001) and Okubo et al. (1997), to be inflated with aqueous pore fluids at pressures significantly above hydrostatic.

Figure 13 looks southwestward down the east rift zone and towards the summit of Kilauea and the subcaldera magma reservoir. MT Line 4 crosses the ERZ orthogonally, and contains beneath it a closed-contour resistivity low of < 5.6 Ω-m. The entire resistivity low extends from about 1.5 to 7 km depth, but it is centered on the 2 to 4 km depth range. This is the centroid of the region of neutral buoyancy for *low-pressure, subcaldera-differentiated* tholeiitic magma (Ryan, 1987a,b), and the generally preferred depth interval for the lateral migration of magma batches within the east rift zone. It is also the preferred depth interval for the storage of (olivine-controlled [Wright, 1971; Wright and Fiske, 1971]) tholeiitic melt, and magma batch mixing concurrent with lateral transport and subvent residence (Garcia et al., 1989; 1992). We interpret the bright orange resistivity low on Line 4 (and the adjacent resistivity low on Line 3) as the *primary* shallow storage region for Pu'u O'o-Kupaianaha magma, prior to vent eruption and subsequent flow towards the ocean. The Okubo et al. (1997) velocity tomogram, also included in Figure 13, has a low-velocity zone at the easternmost extension of the recently active ERZ eruptive vents (coincident with MT Line 4), but does not show low velocities where MT Line 3 and to a lesser extent Line 6 have low resistivity zones at depth beneath the westernmost recently active ERZ surface vents. We speculate that either the spatial resolution of the velocity tomogram in this area is not high enough to distinguish a relatively thin low-velocity zone associated with magma within the solidified higher velocity core of the ERZ, or that the molten zone has increased in size since the time (1986 to 1992) of the data set used by Okubo et al. (1997). In Figure 13, the subcaldera magma reservoir and the conduit into the deeper levels of the volcanic shield may be seen in the distance, beneath and slightly displaced to the south of the junction of the southwest and east rift zones, as illustrated on MT Line 1.

SUMMARY AND CONCLUSIONS

This paper reports the first successful inversion of magnetotelluric [MT] data to recover the two-dimensional resistivity structure of Kilauea Volcano. In this first phase of an ongoing experiment, we have resolved regions of contrasting resistivity beneath the summit caldera, the east rift zone, and the uppermost portion of the southwest rift zone. Experimental challenges included dealing successfully with extremely high contact resistances on fresh lava flows and logistical issues related to access to rough, heavily-faulted, and/or densely-vegetated terrain. Interpretation and data processing issues included dealing with oceanic coastal effects and the effects of topography in model development.

The study has inverted MT data for 33 stations arrayed primarily in six major transects over Kilauea's surface. These six lines are divided broadly into summit-crossing, rift zone-crossing, and rift zone-parallel transects. After inversion, the collected six 2-D MT cross-sections have been assembled in fence diagrams, linked to the volcanic topography and structure, and viewed in three-dimensional perspectives. We have resolved the following five structural and process domains within Kilauea:

(1) *Magma ascent conduit*. Seen as a slightly southward-dipping region of low resistivity, the conduit-like region has a central core where resistivities are <5.6 Ω-m. It is in essential congruence with the upper portions of the primary conduit of Ryan (1988).

(2) *Subcaldera magma reservoir*. Lying beneath the junction of Halemaumau's substructure and the upper southwest rift zone, and occupying the 1.2 km to 3 km depth interval, this

region–in aggregate–is less than 5 Ω-m in its core and is inferred to be comprised of stored magma, subsolidus country rock blocks, and mantling hydrothermal fluids. It corresponds spatially with the uppermost magma-inflated sills of the subcaldera magma reservoir as resolved in Ryan et al. (1983), and to the western and southwestern domains of low V_p in the tomographic study of Dawson et al. (1999).

(3) *East rift zone magma storage beneath the Pu'u O'o-Kupaianaha vent region.* Resolved as closed-contour resistivity lows (5-10 Ω-m), this region is coincident with the tholeiitic horizon of neutral buoyancy (Ryan, 1987a, b) and lies beneath the eruptive vents in the Pu'u O'o-Kupaianaha sector of the east rift zone. It is physically interpreted to consist of a relatively narrow but vertically extensive (2 to 4 km depth) region of magma and country rock blocks, which collectively function as a local storage reservoir for the Phase 4-to-present series of east rift zone eruptions.

(4) *Groundwater and low temperature hydrothermal regions within the Kaoiki fault zone.* Internal to the core of the Kaoiki fault zone, and lying at a depth of 1.5 to 4 km, are a pair of resistivity lows (5-17 Ω-m) that are interpreted as the conductive fault zone core produced by aqueous pore fluids occupying the fractures and microporosity of this basalt sequence. Somewhat analogous to fluids in the Keller-NSF research drill hole (Zablocki et al., 1974), these waters are inferred to have a moderately elevated electrolite content and reside in zeolite-facies altered basalt.

(5) *Hydrothermal regions within the Hilina fault zone.* Resolved in the cross-section of MT Line 2 as a pair of bright orange-red closed-contour resistivity lows (1.77 to 1.0 Ω-m), these regions occupy the Hilina fault zone in the 1–3 km and the $1–6^+$ km depth region, respectively. While far removed from *direct* connections with magma, the regions are about

midway in the interval between the heat sources of stored magma to the north and the sea water of the ocean coast to the south. We posit that blends of sea water (0.333 Ω-m) and meteoric water are being advected vertically upwards within the core of the Hilina fault zone, providing a relatively conductive pathway for electrical currents within the south flank of the volcano.

The 2-D imaging done to date on this data set and its correlations with previous work illustrate that MT data can provide structural information about the magma transport and storage regions of an active volcano, and their hydrothermal surroundings. This work forms an intriguing opening to continued work, in which interpretations will be augmented by lower frequencies and full three-dimensional inversions. Future MT data acquisition will improve the spatial coverage and allow better definition of the lateral distribution of melt and hydrothermal fluids within Kilauea's east rift zone, as well as further definition of the anomalous domains seen in the vicinity of the Hilina fault zone.

ACKNOWLEDGEMENTS

Support for this work was provided by the U.S. Department of Energy under Contract No. DE–AC03–76SF00098. We thank the staff of the Hawaiian Volcano Observatory of the U.S. Geological Survey, U. S. Department of the Interior, for logistical and personnel support, where Arnold T. Okamura helped in many ways. Helicopter support was provided by Volcano

Helicopters/David Okita. Experiments were conducted within the Hawai'i Volcanoes National Park, U.S. National Park Service, U.S. Department of the Interior, and we thank the Hawai'i Volcanoes National Park for their cooperation and support.

REFERENCES

Almendros, J., B.A. Chouet, and P. Dawson, Spatial extent of a hydrothermal system at Kilauea Volcano, Hawaii, determined from array analyses of shallow long-period seismicity. 2. Results. *J. Geophys. Res*. **106**, No. B7, 13,581-13,597, 2001.

Anderson, L.A., Geoelectric character of Kilauea Iki lava lake crust. *in* (Decker, R.W., T.L. Wright, and P.H. Stauffer, Eds.) *Volcanism in Hawaii*. Vol. II. U.S. Geological Professional Paper 1350. 1345-1355, 1987.

Bartel, L. C., and R.D. Jacobson, Results of a controlled-source audiofrequency Magnetotelluric survey at the Puhimau thermal area, Kilauea Volcano, Hawaii. *Geophysics*, **52**, 665-667, 1987.

Berryman, J.G., Mixture theories for rock properties. *in* (T.J. Ahrens, Ed.) *Rock Physics and Phase Relations: A Handbook of Physical Constants*. Vol. III. American Geophysical Union. Washington, D.C., 205-228, 1995.

Budiansky, B. and R.J. O`Connell, Elastic moduli of dry and saturated cracked solids. *Int. J. Solids and Structures.* **12**, 81-97, 1976.

Clague, D.A., J.G. Moore, J.E. Dixon, and W.B. Friesen, Petrology of submarine lavas from Kilauea'sPuna Ridge, Hawaii. *J. Petrology*, **36**, No.2, 299-349, 1995.

Dawson, P.B., B.A. Chouet, P.G. Okubo, A. Villasenor, and H. M. Benz, Three-dimensional velocity structure of the Kilauea Caldera, Hawaii, *Geophys. Res. Lett.,* **26**, 2805-2808, 1999.

Easton, R. M., Stratigraphy of Kilauea Volcano. *in* (R.W. Decker, T.L. Wright, and P.H. Stauffer, Eds.) *Volcanism in Hawaii.* Vol.I . U.S. Geological Survey Professional Paper 1350. 243-260., 1987.

Egbert, G.D., Robust multiple-station magnetotelluric data processing, *Geophys. J. Int.,* **130**, 475-496, 1997.

Flanigan, V. and C.L. Long, Aeromagnetic and near-surface electrical expression of the Kilauea amd Mauna Loa volcanic rift systems. *in* (R.W. Decker, T.L. Wight, and P.H. Stauffer, Eds.) *Volcanism in Hawaii.* Vol. II. U.S. Geological Professional Paper 1350, 935-946, 1987.

Fournier, R.O., Conceptual models of brine evolution in magmatic-hydrothermal systems. *in* (R.W. Decker, T.L. Wright, and P.H. Stauffer, Eds.) *Volcanism in Hawaii.* Vol.II. U.S. Geological Professional Paper 1350. 1,487-1,506, 1987.

Frantz, J.D., J. Dubessy, and B.O. Mysen, An optical sell for Raman spectroscopic studies of supercritical fluids and its application to the study of water to 500°C and 2,000 bar. *Chemical Geology*. **106**, 9-26, 1993.

Frantz, J.D. and W.L. Marshall, Electrical conductances and ionization constants of Calcuim Chloride and Magnesium Chloride in aqueous solutions at temperatures to 600°C and pressures to 4,000 bars. *American J. of Science.* **282**, 1.666-1,693, 1982.

Gamble, T.D., W.M. Goubau, and J. Clarke, Magnetotellurics with a remote magnetic reference, *Geophysics*, **44**, 53-68, 1979.

Garcia, M.O., R.A. Ho, J.M. Rhodes, and E.W. Wolfe, Petrologic constraints on rift-zone processes: Results from episode 1 of the Puu Oo eruption of Kilauea volcano, Hawaii. *Bull. Volcanol*., **52**, 81-96, 1989.

Garcia, M.O., J.M. Rhodes, E.W. Wolfe, G.E. Ulrich, and R.A. Ho, Petrology of lavas from episodes 2-47 of the Puu Oo eruption of Kilauea Volcano, Hawaii: Evaluation of magmatic processes. *Bull. Volcanol*., **55**, 1-16, 1992.

Gasperikova, E., Hoversten, G.M., Ryan, M.P., Kauahikaua, J.P., Newman, G.A., and Cuevas, N., Magnetotelluric investigations of Kilauea volcano, Hawai'i. Part I: Experiment design and data processing. *Journal of Geophysical Research*, this issue, 2003.

Haslinger, F., C. Thurber, M. Mandernach, and P. Okubo, Tomographic image of P-velocity structure beneath Kilauea'sEast Rift Zone and South Flank: Seismic evidence for a deep magma body, *Geophys. Res. Lett.,* **28**,. 375-378, 2001.

Hermance, J.F., An electrical model for the sub-Icelandic crust. *Geophysics.* **38**, No. 1, 3-13, 1973.

Hermance, J.F., Electrical conductivity models of the crust and mantle. *in* (T.J. Ahrens, Ed.) *Global Earth Physics: A Handbook of Physical Constants*. Vol. I. American Geophysical Union. Washington, D.C., 190-205, 1995.

Holcomb, R.T., Eruptive history and long-term behavior of Kilauea Volcano. *in* (R.W. Decker, T.L. Wright, and P.H. Stauffer, Eds.) *Volcanism in Hawaii.* Vol.I. U.S. Geological Survey Professional Paper 1350, 261-350, 1987.

Jackson, D.B., J. P. Kauahikaua, and C.J. Zablocki, Resistivity monitoring of an active volcano using controlled-source electromagnetic technique: Kilauea, Hawaii, *J. Geophys. Res.,* **90**, 12,545-12,555, 1985.

Kauahikaua, J.P., D.B. Jackson and C.J. Zablocki, Resistivity structure to a depth of 5 km beneath Kilauea Volcano, Hawaii from large-loop-source electromagnetic measurements (0.04-8 Hz), *J. Geophys. Res.,* **91**, 8,267-8,283, 1986.

Kauahikaua, J.P., T. Hildenbrand, and M. Webring, Deep magmatic structures of Hawaiian volcanoes, images by three-dimensional gravity models*, Geology*, **28**, 883-886, 2000.

Klein, F.W., R.Y. Koyanagi, J.S. Nakata, and W.R. Tanigawa, The seismicity of Kilauea'smagma system, *in* (Decker, R.W., T.L. Wright, and P.H. Stauffer, Eds.) *Volcanism in Hawaii.* Vol. II. U.S. Geological Survey Professional Paper 1350, 1,019-1,186, 1987.

Llera, F.J., M. Sato, K. Nakatsuka, and H. Yokoyama, Temperature-dependence of the electrical resistivity of water-saturated rocks. *Geophysics,* **55**, No. 5; 576-585, 1990.

Lockwood, J.P., and P.W. Lipman, Holocene eruptive history of Mauna Loa Volcano. *in* (R.W. Decker, T.L. Wright, and P.H. Stauffer, Eds.) *Volcanism in Hawaii*. Vol. I. U.S. Geological Survey Professional Paper 1350. 509-536, 1987.

Mackie, R.L., B.R. Bennet, and T.R. Madden, Long-period magnetotelluric measurements near the central California coast: A land-locked view of the conductivity structure under the Pacific Ocean, *Geophys. J. Int.,* **95**, 181-194, 1988.

Manghnani, M.H. and C.S. Rai, Electrical conductivity of a spinel lherzolite and a garnet peridotite to 1550 C: Relevance to the effects of partial melting. *Bulletin Volcanologique*.**41**, No. 4, 328-332,1978.

Matsushima, N., H. Oshima, Y. Ogawa, S. Takakura, H. Satoh, M. Utsugi, and Y. Nishida, Magma prospecting in Usu Volcano, Hokkaido, Japan, using magnetotelluric soundings, *J. Volcanology and Geother. Res*., **109**, 263-277, 2001.

Mavko, G.M., Velocity and attenuation in partially molten rocks*, J. Geophys. Res.,* **85**, 5,173-5,189, 1980.

Mavko, G. M., J. Dvorkin, and A. Nur, *The Rock Physics Handbook*: *Tools for seismic analysis in porous media*. Cambridge University Press. Cambridge, England. 329 pp., 1998.

Murase, T. and I. Kushiro, Compressional wave velocity in partially molten peridotite at high pressures. *Yearbook* **77**. *Geophysical Laboratory of the Carnegie Institution of Washington.* 559-562, 1978.

Murase, T. and A.R. McBirney, Properties of some common igneous rocks and their melts at high temperatures. *Geol. Soc. Amer. Bull*., **84**, 3563-3592, 1973.

Newman, G.A., D.L. Alumbaugh, Three-dimensional magnetotelluric inversion using nonlinear conjugate gradients, *Geophys. J. Int.,* **140**, 410-424, 2000.

Newman, G.A., G.M. Hoversten, D.L. Alumbaugh, Three-dimensiomnal magnetotelluric modeling and inversion: Application to sub-salt imaging. *in* (M.S. Zhdanov, Ed.) *Three-*

Dimensional Electromagnetics. Proceedings of the Second International Symposium. Elsevier Science, 127-152, 2002.

Nolasco, R., P. Tarits, J.H. Filloux, and A.D. Chave, Magnetotelluric imaging of the Society Islands hotspot*, J. Geophys. Res*., **103**, 30,287-30,309, 1998.

Ogawa, Y., H.M. Bibby, T.G. Caldwell, S. Takakura, T. Uchida, N. Matsushima, L. Bennie, T. Tosha, and Y. Nishi, Wide-band magnetotelluric measurements across the Taupo Volcanic Zone, New Zealand-preliminary results, *Geophys. Res., Lett.,* **26**, 3,673-3,676, 1999.

Okubo, P.G., H.M. Benz, and B.A. Chouet, Imaging the crustal magma sources beneath Mauna Loa and Kilauea volcanoes, Hawaii, *Geology*, **25**, 867-870, 1997.

Olhoeft, G.R., Electrical properties of water-saturated basalt: Preliminary results to 506 K (233 C). *U.S. Geological Survey Open File Report* 77-688. 3pp; 5 figures, 1977.

Ohminato, T., B.A. Chouet, P. Dawson, and S. Kedar, Waveform inversion of very long-period impulsive signals associated with magmatic injection beneath Kilauea Volcano, Hawaii. *J. Geophys. Res*., **103**, No. B10, 23,839-23,862, 1998.

Orange, A.S., Magnetotelluric exploration for hydrocarbons, *Proc. IEEE,* **77**, 287-318, 1989.

Park, S.K., C. Torres-Verdin, A systematic approach to the interpretation of magnetotelluric data in volcanic environments with applications to the quest for magma in Long Valley, California, *J. Geophys. Res.,* **93**, 13,265-13,283, 1988.

Quist, A.S. and W.L. Marshall, Electrical conductances of aqueous Sodium Chloride solutions from 0 to 800 degrees and at pressures to 4,000 bars. *Journal of Physical Chemistry.* **72**, No. 2, 684-703, 1968.

Rai, C.S. and M.H. Manghnani, Electrical conductivity of basalts to 1550 C. *in* (Dick, H.J.B., Ed.) *Magma Genesis*. Proceedings of Chapman Conference: Partial Melting in the Earth`s Mantle. Oregon Department of Geology and Mineral Industries Bulletin **96**, 219-232, 1977.

Rai, C.S. and M.H. Manghnani, Electrical conductivity of ultramafic rocks to 1820 Kelvin. *Physics of the Earth and Planetary Interiors*. **17**, 6-13, 1978.

Rai, C.S., and M.H. Manghnani, The effects of saturant salinity and pressure on the electrical resistivity of Hawaiian basalts. *Geophys. J. Royal Astr. Soc.,* **65**, 395-405, 1981.

Rodi, W. and R.L. Mackie, Nonlinear conjugate gradients algorithm for 2-D magnetotelluric inversion, *Geophysics*, **66**, 174-187, 2001.

Ryan, M.P., Mechanical behavior of magma reservoir envelopes: Elasticity of the olivine tholeiite solidus. Bull. Volcanologique. **43-4,** 743-772, 1980.

Ryan, M.P., The elasticity and contractancy of Hawaiian olivine tholeiite, and its role in the structural evolution of subcaldera magma reservoirs and rift systems. *in* (Decker, R.W., T.L. Wright, and P.H. Stauffer, Eds.) *Volcanism in Hawaii.* Vol.II. U.S. Geological Survey Professional Paper 1350. 1395-1447,1987a.

Ryan, M.P., Neutral buoyancy and the mechanical evolution of magmatic systems. *in* (B.O. Mysen, Ed.) *Magmatic Processes: Physicochemical Principles*. The Geochemical Society. Special Publication No. 1., 259-287, 1987b.

Ryan, M.P., The mechanics and three-dimensional internal structure of active magmatic systems: Kilauea volcano, Hawaii. *J. Geophys. Res*. **93**, No. B5, 4,213-4,248,1988.

Ryan, M.P., J.Y.K. Blevins, A.T. Okamura, and R.Y. Koyanagi, Magma reservoir subsidence mechanics: Theoretical summary and application to Kilauea volcano, Hawaii. *J. Geophys. Res.* **88**, 4,147-4,181, 1983.

Ryan, M.P., R.Y. Koyanagi and R.S. Fiske, Modelling the three-dimensional structure of macroscopic magma transport systems: Application to Kilauea volcano, Hawaii. *J. Geophys. Res*. **86**, 7,111-7,129, 1981.

Saccorotti, G., B.A. Chouet, and P. Dawson, Wavefield properties of a shallow long-period event and tremor at Kilauea Volcano, Hawaii. *Journal of Volcanology and Geothermal Research*. **109**, 163-189, 2001.

Santos, F.A., M.M. Nolasco, E.P. Almeida, J. Pous, and L.A. Mendes-Victor, Coast effects on magnetic and magnetotelluric transfer functions and their correction: Application to MT soundings carried out in SW Iberia, *Earth and Planetary Sci. Lett.,* **186**, 283-295, 2001.

Takasaki, K.J., Summary appraisals of the nation`s ground water resources--Hawaii region. U.S. Geological Survey Professional Paper 813-M, 175pp., 1978.

Takei, Y., Constitutive mechanical relations of solid-liquid composites in terms of grain-boundary contiguity, *J. Geophys. Res.,* **103**, 18,183-18,203, 1998.

Thomas, D.M., A geochemical model of the Kilauea East Rift Zone. *in* (R.W. Decker, T.L. Wright, and P.H. Stauffer, Eds.). *Volcanism in Hawaii*. Vol. II. U.S. Geological Survey Professional Paper 1350. 1507-1525, 1987.

Tyburczy, J.A. and D.K. Fisler, Electrical properties of minerals and melts. *in* (T.J. Ahrens, Ed.) *Mineral Physics and Crystallography: A handbook of Physical Constants*. Vol. II. American Geophysical Union. Washington, D.C., 185-208, 1995.

Tyburczy, J.A. and Waff, H.S., Electrical conductivity of molten basalt and andesite to 25 kilobars pressure: Geophysical significance and implications for charge transport and melt structure. *J. Geophys. Res.* **88**, No. B3, 2,413-2,430, 1983.

Tyburczy, J.A. and H.S. Waff, High pressure electrical conductivity in naturally occurring silicate liquids. in (R.N. Schock, Ed.) *Point Defects in Minerals.* Geophysical Monograph 31. Mineral Physics monograph 1. American Geophysical Union. Washington, D.C., 78-87, 1985.

Ucok, H., I. Ershaghi, and G.R. Olhoeft, Electrical resistivity of geothermal brines. *Journal of Petroleum Technology*, April, 717-727, 1980.

Vozoff, K., The magnetotelluric method. *in*: *Electromagnetic Methods in Applied Geophysics*, Vol. 2. Society of Exploration Geophysicists, SEG, 641-712, 1996.

Walker, G.P.L, The dike complex of Koolau volcano, Oahu: Internal structure of a Hawaiian rift zone. *in* (Decker, R.W., T.L. Wright, and P.H. Stauffer, Eds.) *Volcanism in Hawaii.* Vol. II. U.S. Geological Survey Professional Paper 1350. 961-993, 1987.

Walsh, J. B., New analysis of attenuation in partially melted rock. *J. Geophys. Res.,* **74**, 4,333-4,337, 1969.

Wright, T.L, Chemistry of Kilauea and Mauna Loa lava in space and time. U.S. Geological Survey Professional Paper 735. 40 pp., 1971.

Wright, T.L. and R.S. Fiske, Origin of the differentiated and hybrid lavas of Kilauea Volcano, Hawaii. *J. Petrology*. **12**, No.1, 1-65, 1971.

Wyss, M., F. Klein, K. Nagamine, and S. Wiemer, Amonalously high *b*-values in the south flank of Kilauea volcano, Hawaii: Evidence for the distribution of magma below Kilauea'sEast Rift Zone. *Journal of Volcanology and Geothermal Research*. **106,** 23-37, 2001.

Zablocki, C.J., R.I. Tilling, D.W. Peterson, R.L. Christiansen, G.V. Keller, and J.C. Murray, A deep research drill hole at the summit of an active volcano, *Geophys. Res. Lett.,* **1**, 323-326, 1974.

Zohdy, A.A.R. and D.B. Jackson, Application of deep electrical soundings for groundwater exploration in Hawaii. *Geophysics,* **40**, 584-600, 1969.

FIGURE CAPTIONS

Figure 1. Magnetotelluric [MT] survey location map in relationship to Kilauea Volcano and its summit caldera and rift zones. MT data have been acquired at stations shown as blue triangles. Some surface vents active since the onset of the Pu'u O'o–Kupaianaha series of eruptions (from January 3, 1983) are shown in green within the east rift zone.

Figure 2. (a) Z_{xy} and Z_{yx} phase for the Keller-NSF site; (b) Z_{xy} and Z_{yx} apparent resistivity at the Keller-NSF site; (c) Z_{xy} and Z_{yx} phase for site S05; (d) Z_{xy} and Z_{yx} apparent resistivity at site S05. The x-axis is oriented positive to the east with the y-axis oriented positive to the south. Recording time was 72 hours for the Keller-NSF site, and 48 hours for site S05.

Figure 3. MT station map with six 2-D MT lines used in the 2-D resistivity inversions. The surface elevation is contoured in meters above sea level. The outline of the region of intense diking, eruptive vents and caldera and rift zone fracturing, is superposed with the projection of the magmatic region of Ryan (1988), and is positioned 1 km beneath the surface (shown in black). Impedance polar diagrams at 0.01 Hz are plotted at selected stations to illustrate the spatial variations in electromagnetic impedance.

Figure 4. Variations in basalt resistivity through the melting interval based on the data of Rai and Manghnani (1977), as modified by Kauahikaua (1982). The total span in temperature is 20° to 1400°C. The two broad U-shaped shaded regions from 20° to >600°C indicate expected ranges

in resistivity for porous basalts with pore fluids of varying salinities. The cusp between ~ 900°C and ~1,100°C is a kinetic artefact of the original Rai and Manghnani (1977) experiments and is indicative of nonequilibrium conditions during the impedance measurement runs. Arrow labeled "melt" has its origin at the 1 atm melting temperature of basalt.

Figure 5. (a) Section plan view (at sea level) of the three-dimensional (3-D) finite difference model of the island of Hawai'i. The rows and columns of the mesh have been refined in the vicinity of Kilauea Caldera and its rift zones, to enhance overall spatial resolution. (b) 3D cut-away view of the finite difference model through Kilauea Volcano and its rift zones, as viewed from the southwest.

Figure 6. MT station map with 3-D numerical impedance polar diagrams at 0.01 Hz plotted at selected sites, for comparison with field data polar diagrams illustrated in Figure 4. Contrast the modeled electromagnetic isotropy in the region of the summit caldera with the measured anisotropy acquired in the field experiment.

Figure 7. Two-dimensional MT inverse resistivity section beneath Line 1. Data is limited to frequencies greater than 0.01 Hz to eliminate topographic and coastal effects.

Figure 8. Apparent resistivity (upper nine plots) and phase (lower nine plots) for Z_{XY} mode on survey Line 1. Field data are black error bar symbols; the calculated responses of the final inverse model (Figure 7) are shown as red lines.

Figure 9. Two-dimensional resistivity images from Lines 1 and 6. The projected outline of the magmatic regions, including the zone of intense diking, surface venting, and rift zone fracturing, is illustrated in black outline and is from Ryan (1988), positioned at a depth of 1 km. Regions of low resistivity and anomalously high V_P/V_S (Dawson et al., 1999) are interpreted as magma-impregnated.

Figure 10. Three-dimensional configuration of regions of contrasting resistivity as viewed from the south-southwest. Profiles A-A' and B-B' are from Haslinger et al. (2001), and illustrate regions of high b-values (Wyss et al., 2001) and inferred high aqueous fluid pore pressures well south of the east rift zone axis. Blues on seismic velocity profiles are high velocity, whereas reds are regions of low velocity.

Figure 11. Three-dimensional view from the northwest illustrating all six survey lines and the 2-D MT inverse resistivity sections beneath them. Surface vents active since the inception of the Pu'u O'o eruptive series are illustrated in yellow. Kilauea Caldera and the magmatic intrusion regions above rift zones and subcaldera storage regions are shown in black outline (Ryan, 1988). MT station locations are filled black circles.

Figure 12. Three-dimensional view of resistivity fence diagrams, as viewed from the south-southwest. Included is a 1–3 km depth slice from the compressional wave tomographic study of Okubo et al. (1997). The Kaoiki fault zone and the Hilina fault system appear as low resistivity

(red) and relatively low V_p (red) regions within the respective vertical electromagnetic sections and horizontal velocity slice.

Figure 13. Three-dimensional view of Kilauea from the northeast, illustrating the electrical resistivity fence diagrams in combination with the 5–7 km depth slice of Okubo et al. (1997). Note the large low-resistivity zone dipping to the south beneath Line 4, where compressional wave velocities are anomalously low. However, the large resistivity low resolved on Line 3 (beneath the vicinity of the Pu'u O'o vents) does not correlate with the relatively high V_p values inferred from the study of Okubo et al. (1997).

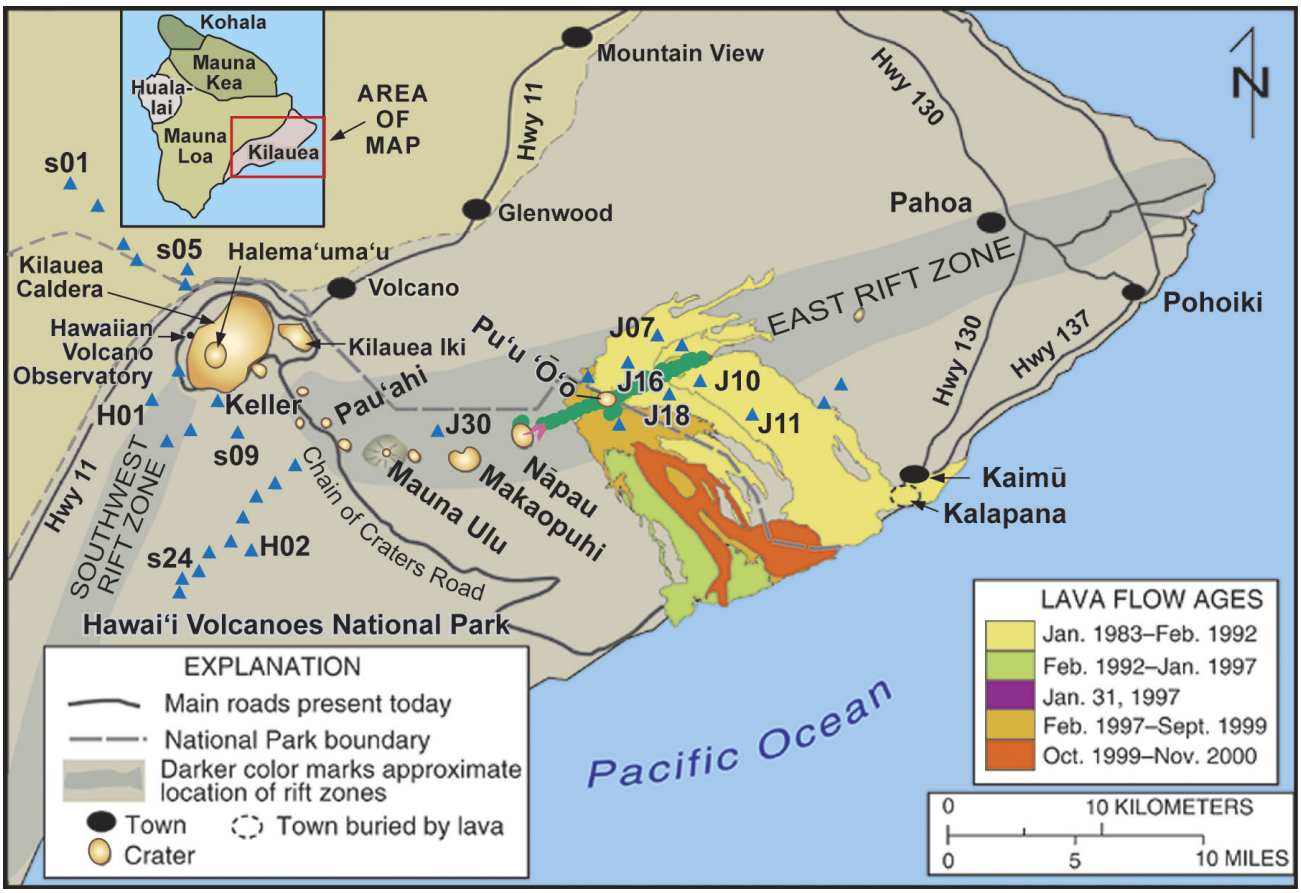

Hoversten et al., Figure 1

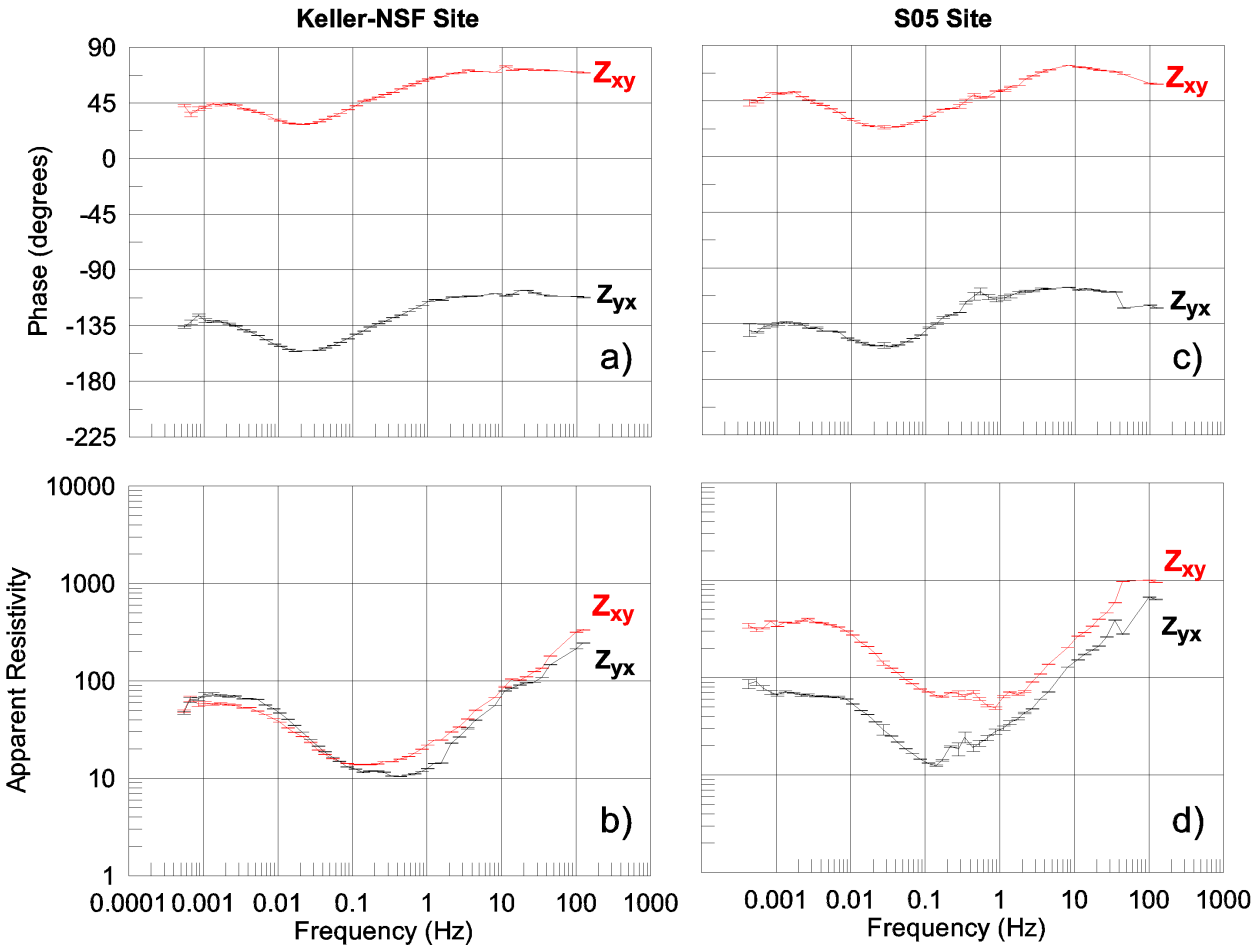

Hoversten et al., Figure 2

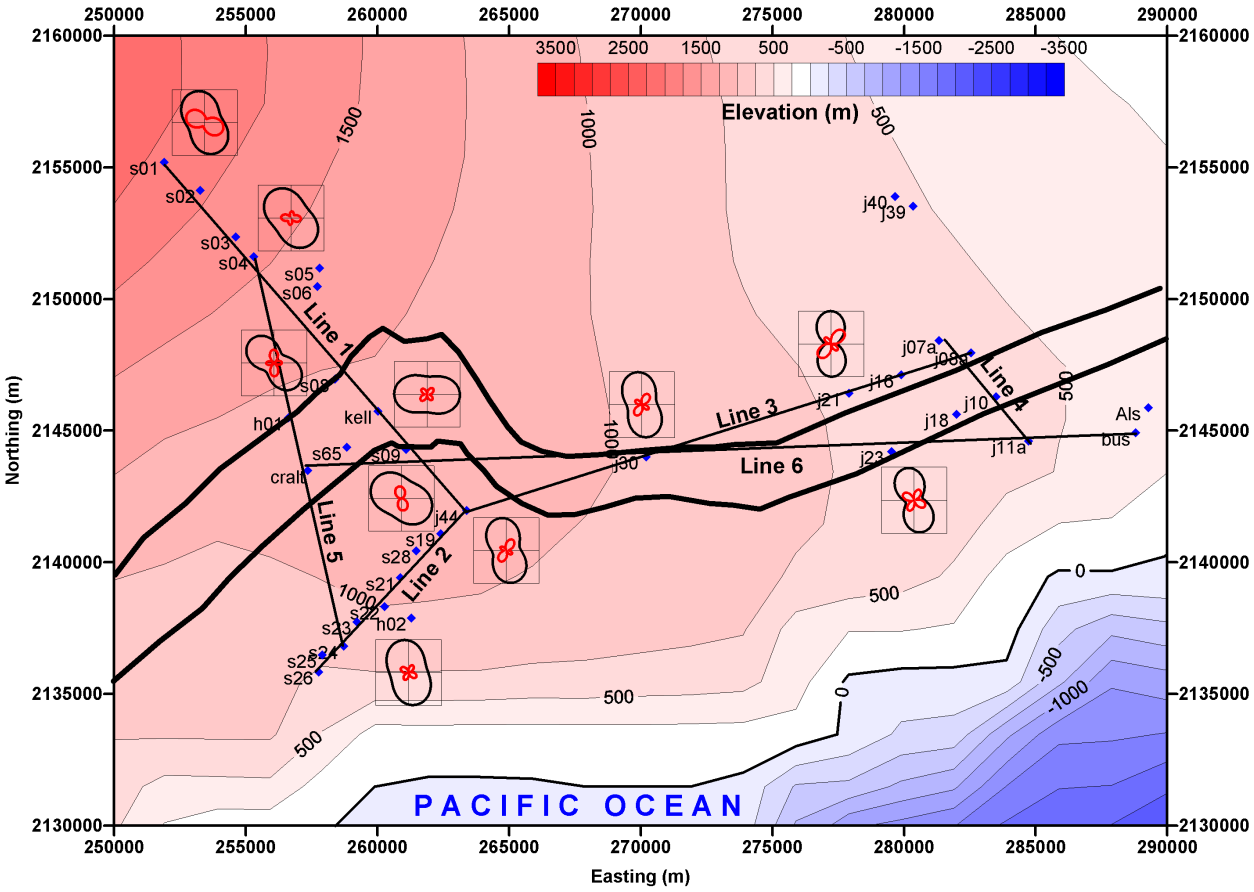

Hoversten et al., Figure 3

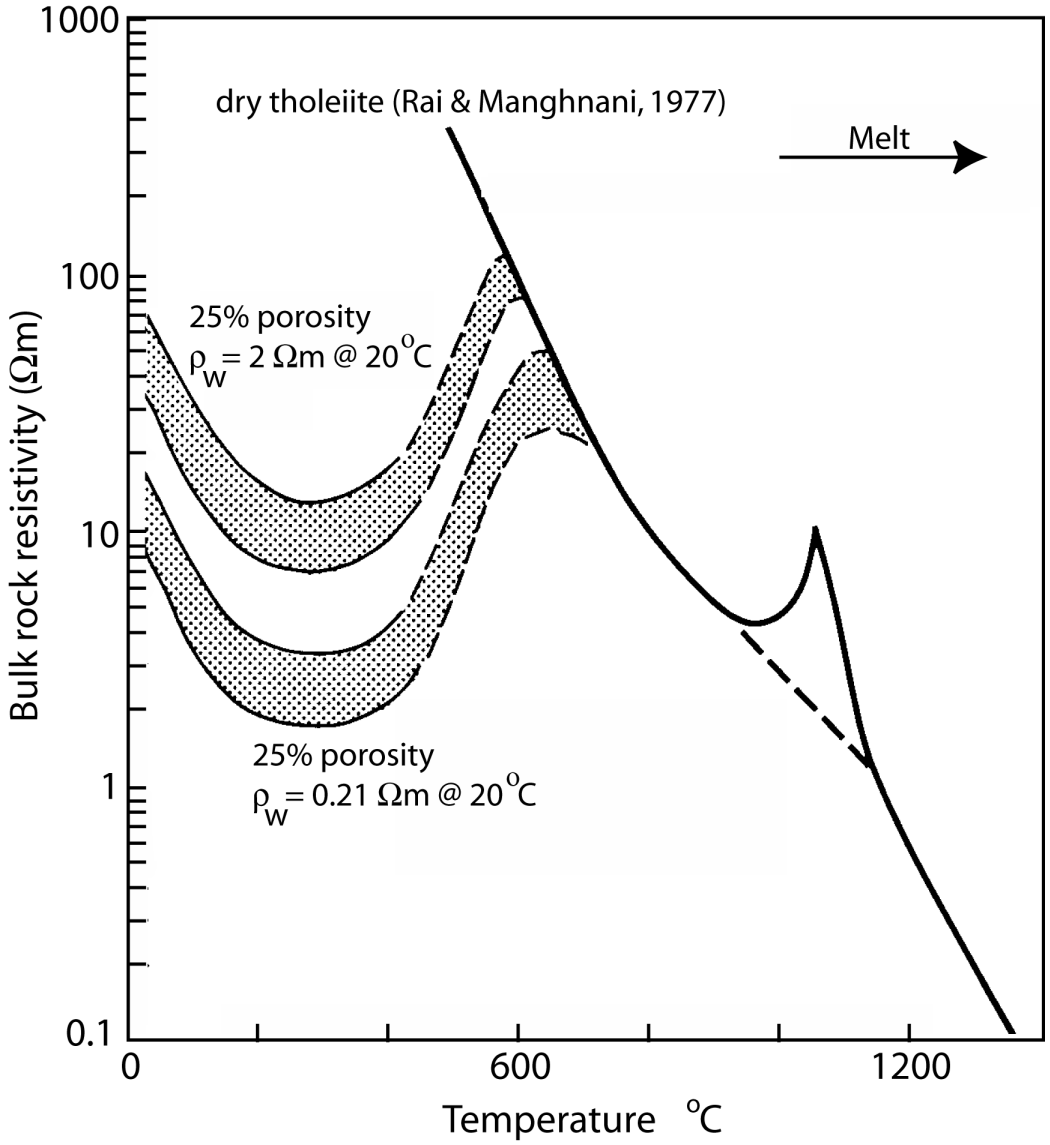

Hoversten et al., Figure 4

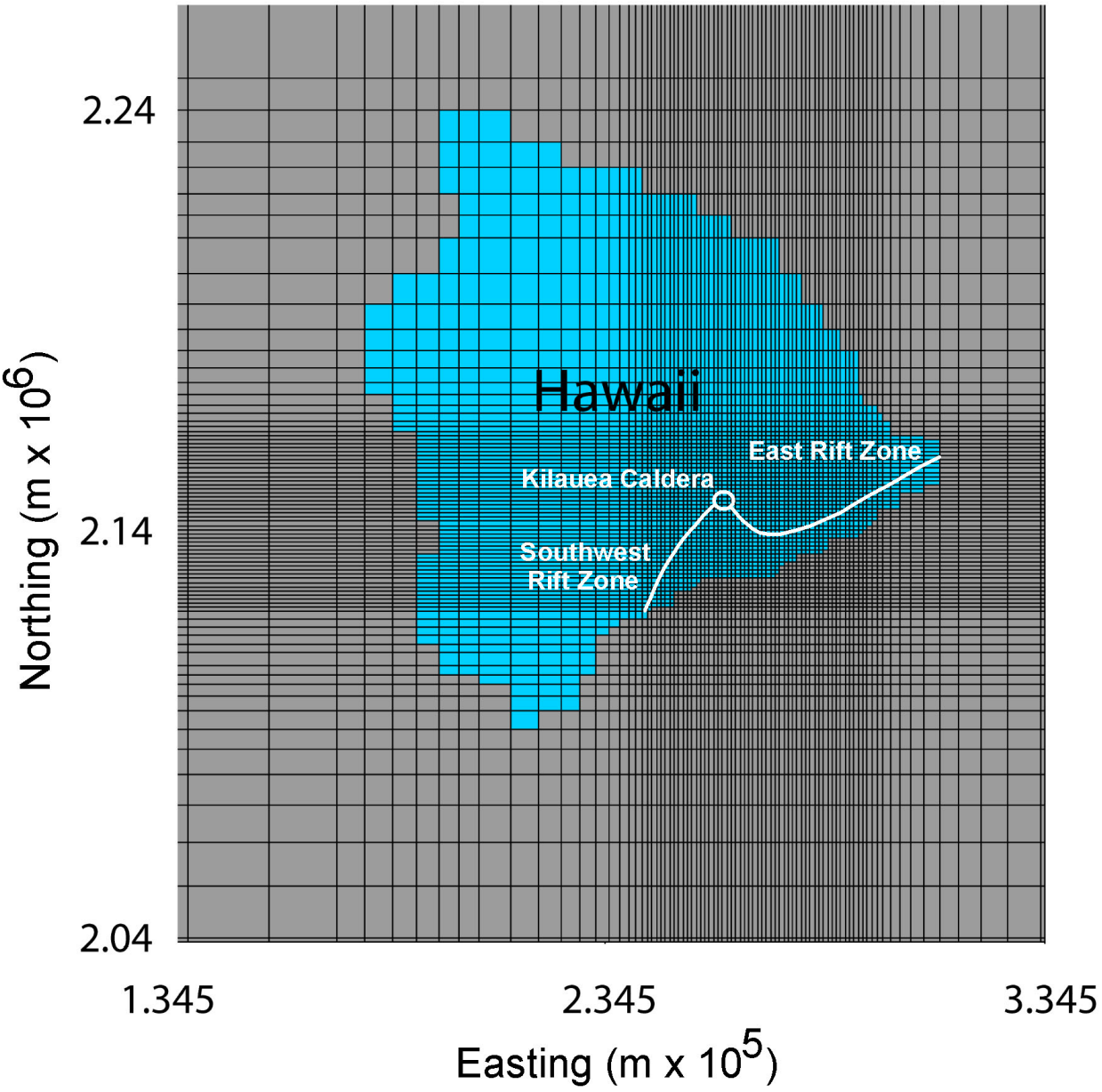

Hoversten et al., Figure 5a

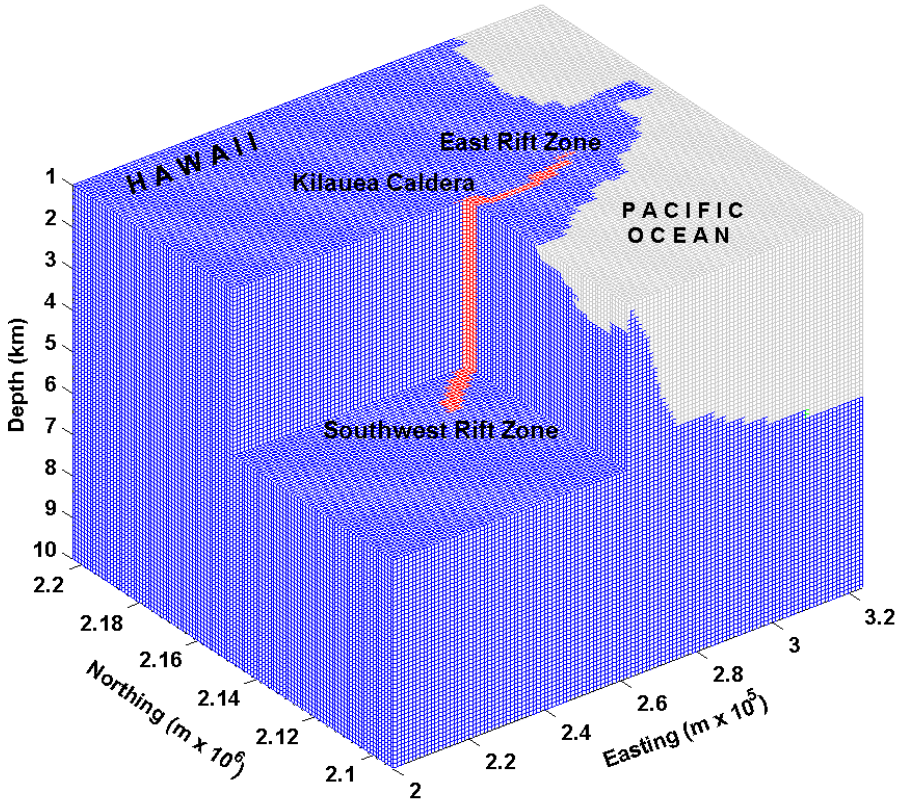

Scale = 1:1:10

Hoversten et al., Figure 5b

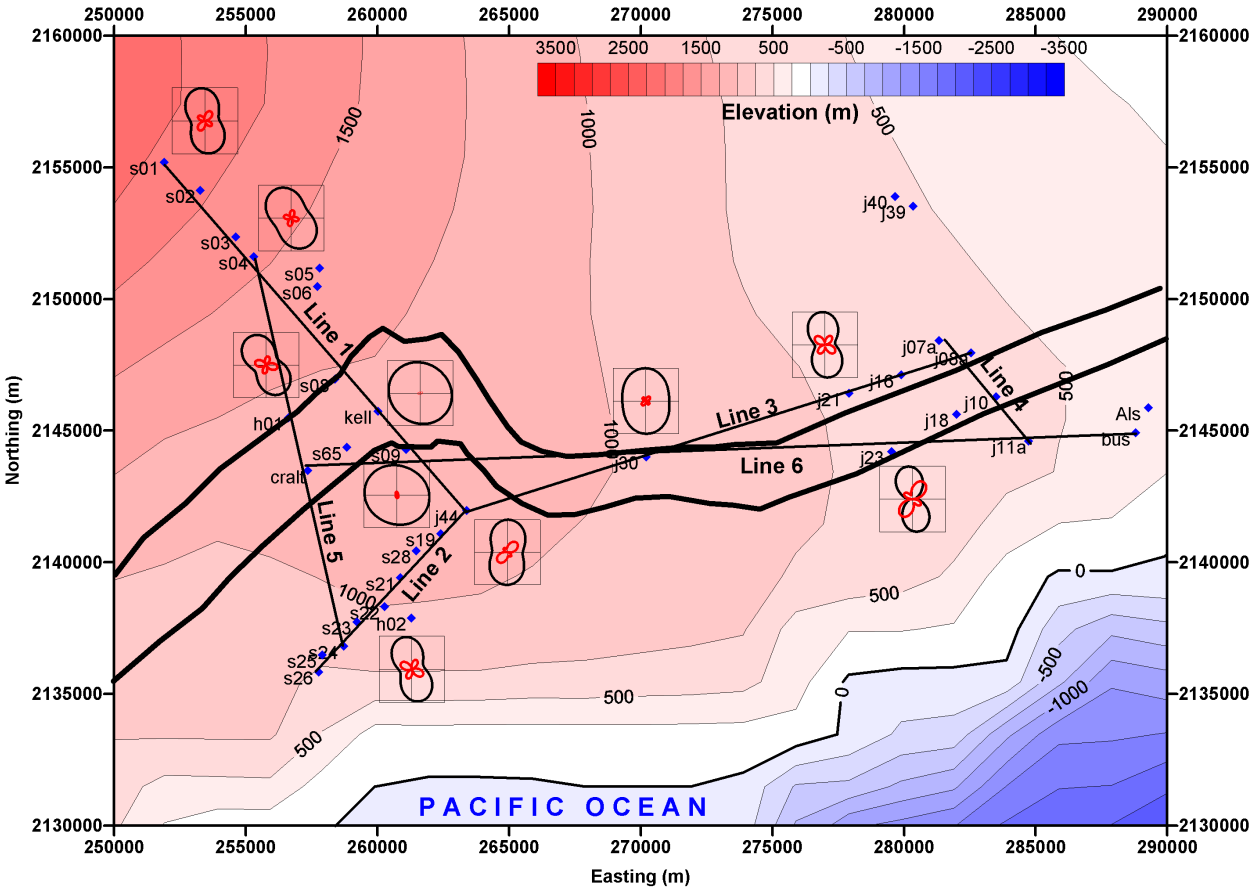

Hoversten et al., Figure 6

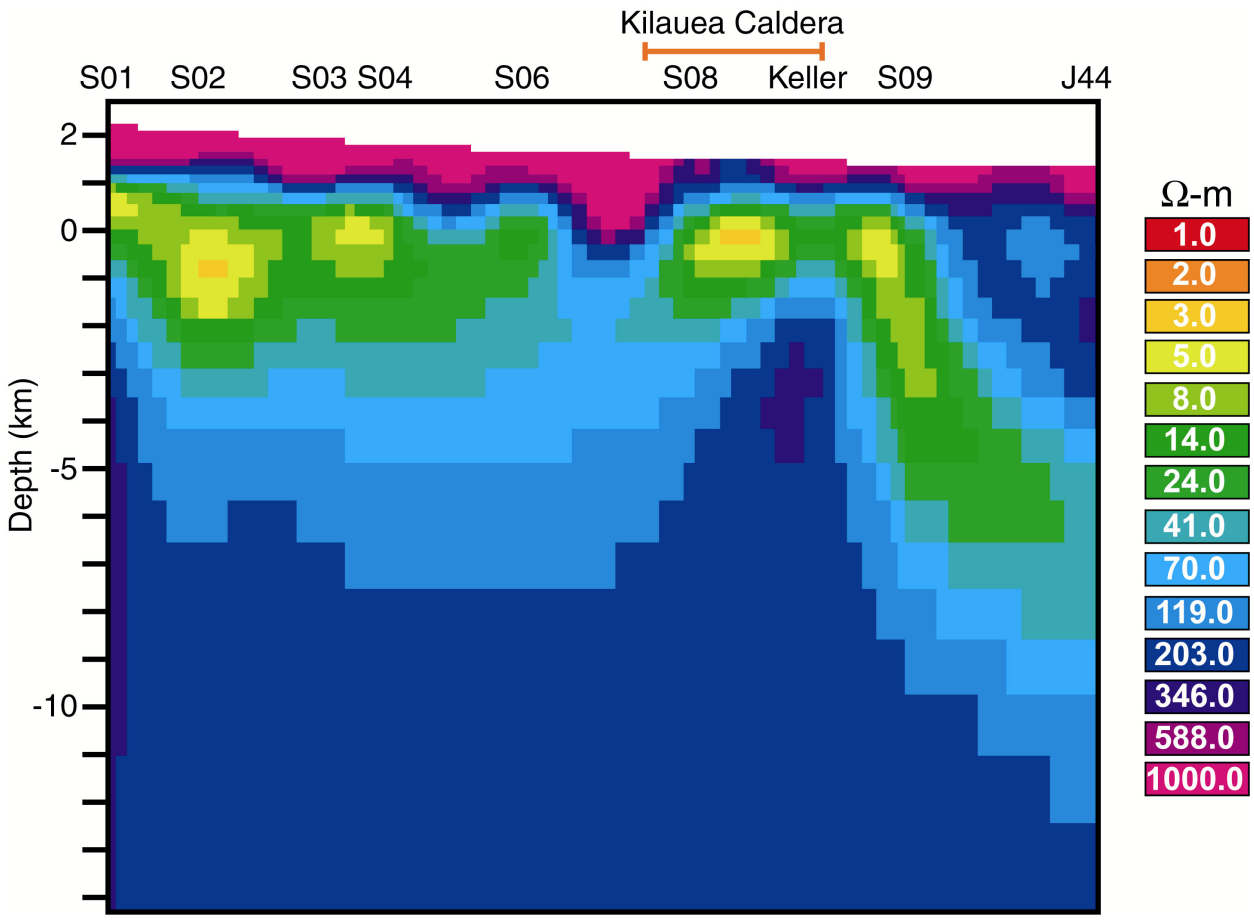

Hoversten et al., Figure 7

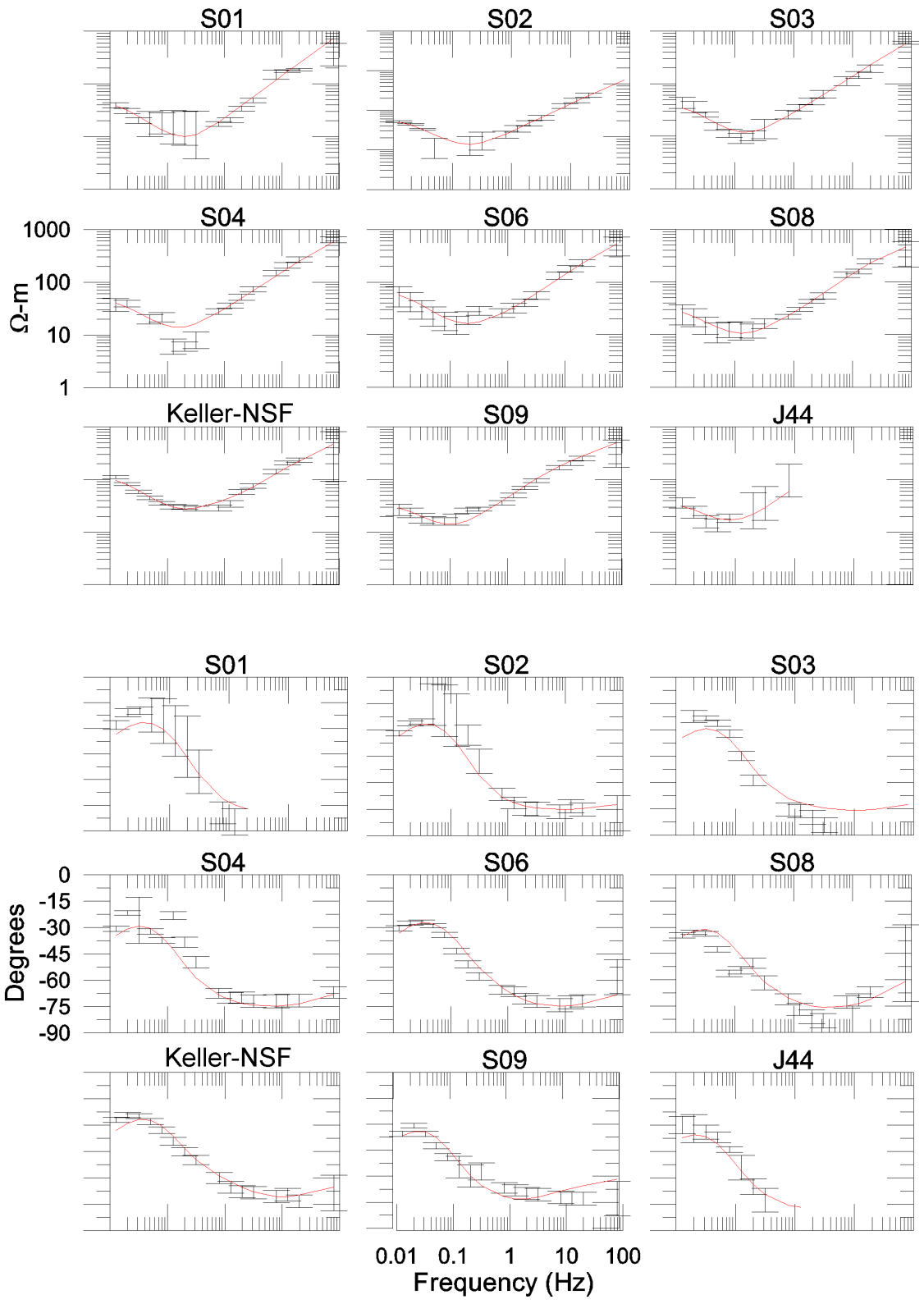

Hoversten et al., Figure 8

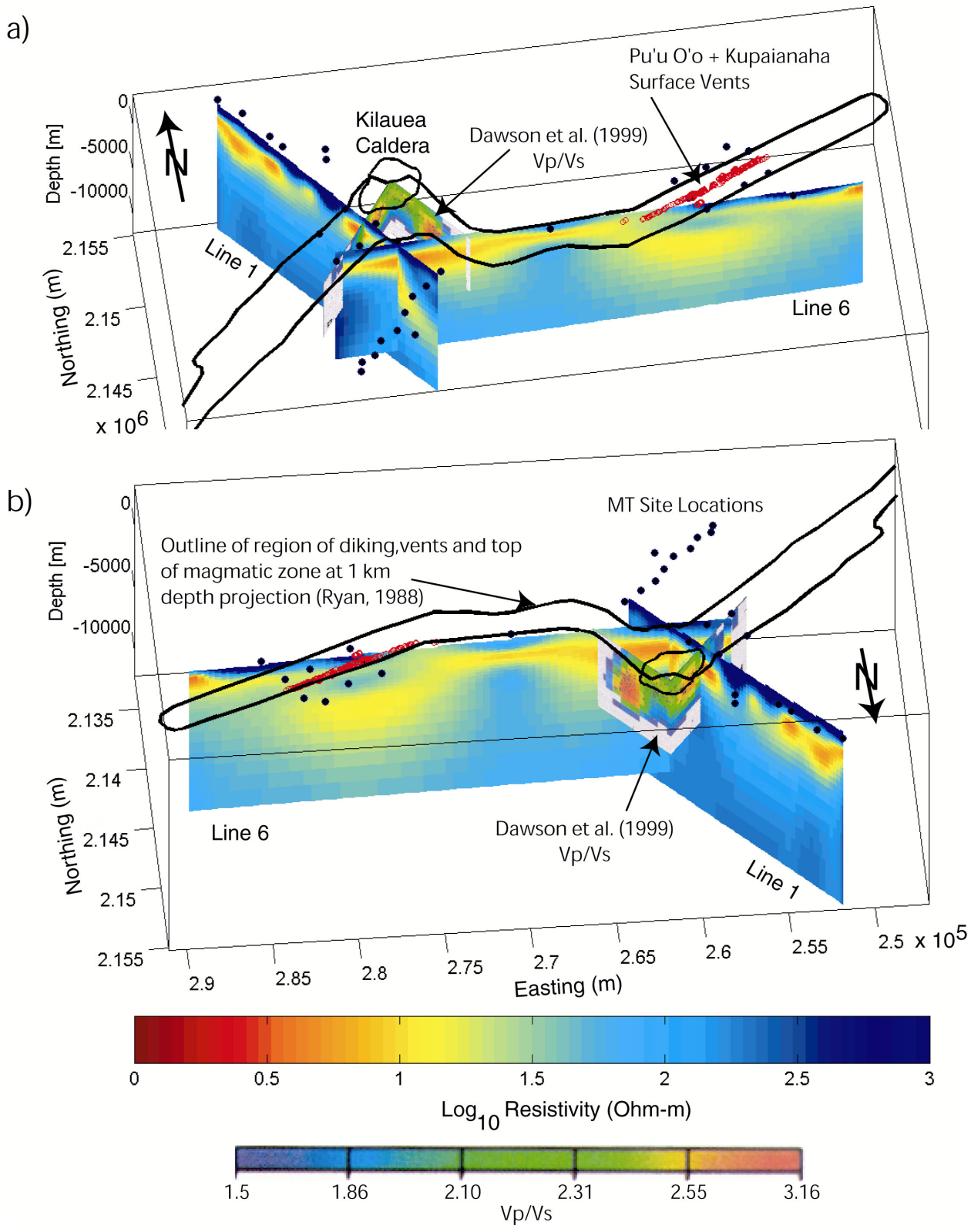

Hoversten et al., Figure 9

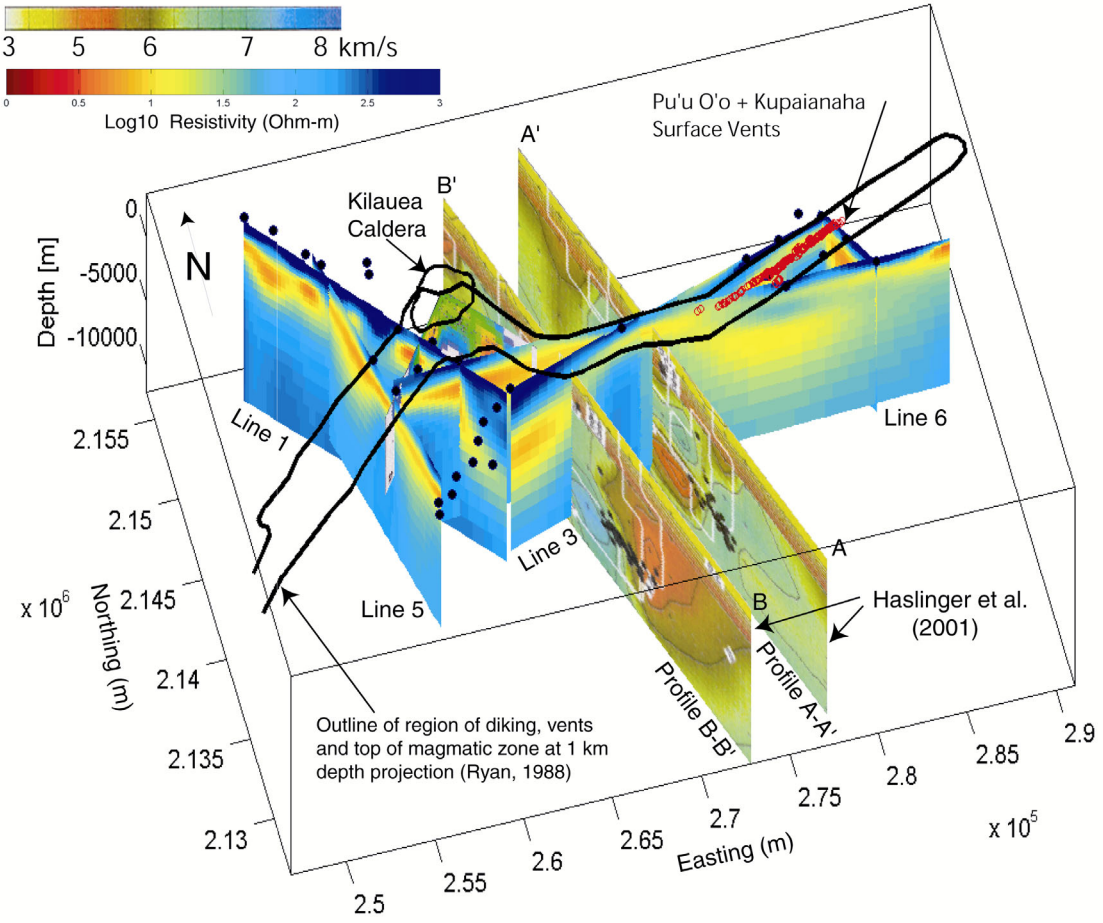

Hoversten et al., Figure 10

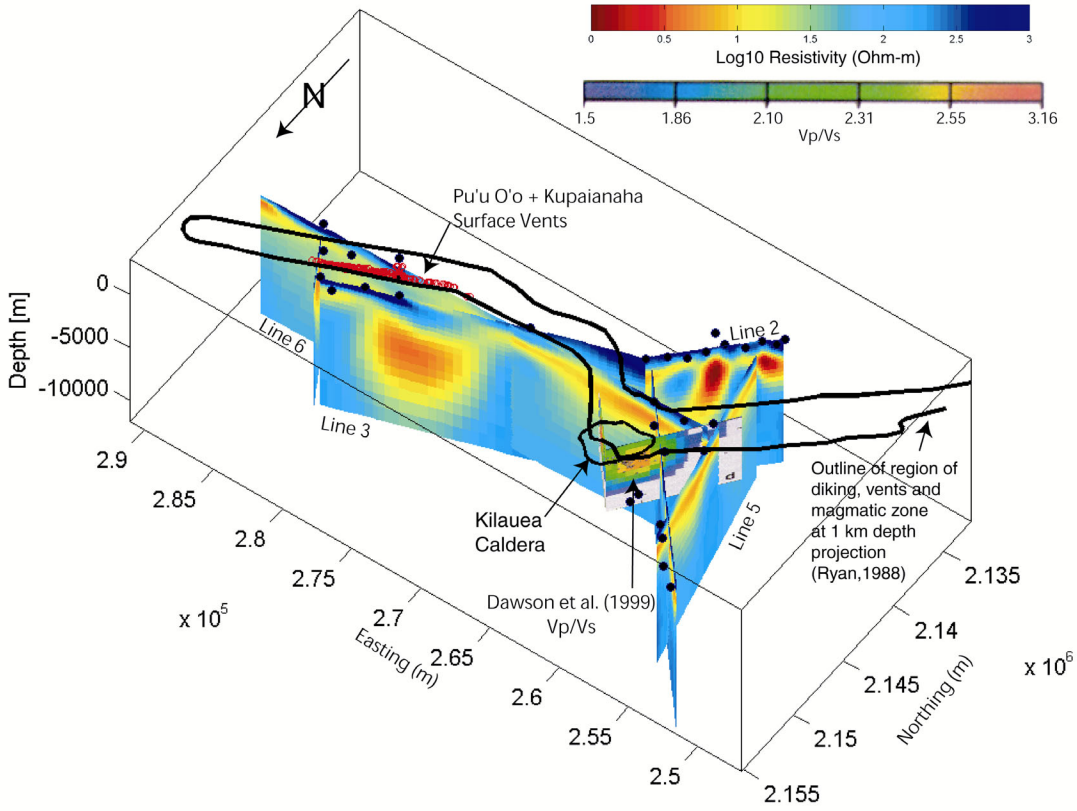

Hoversten et al., Figure 11

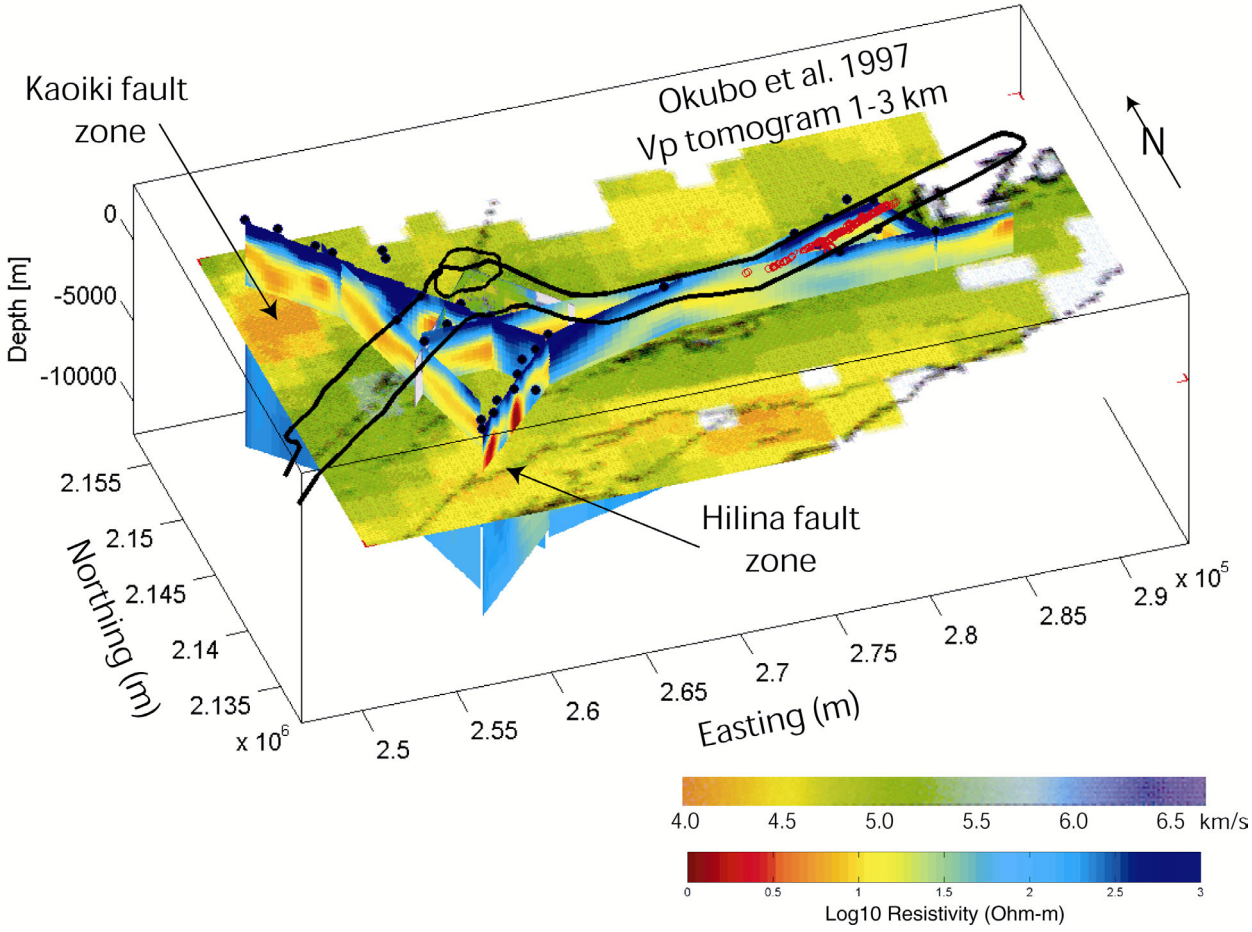

Hoversten et al., Figure 12

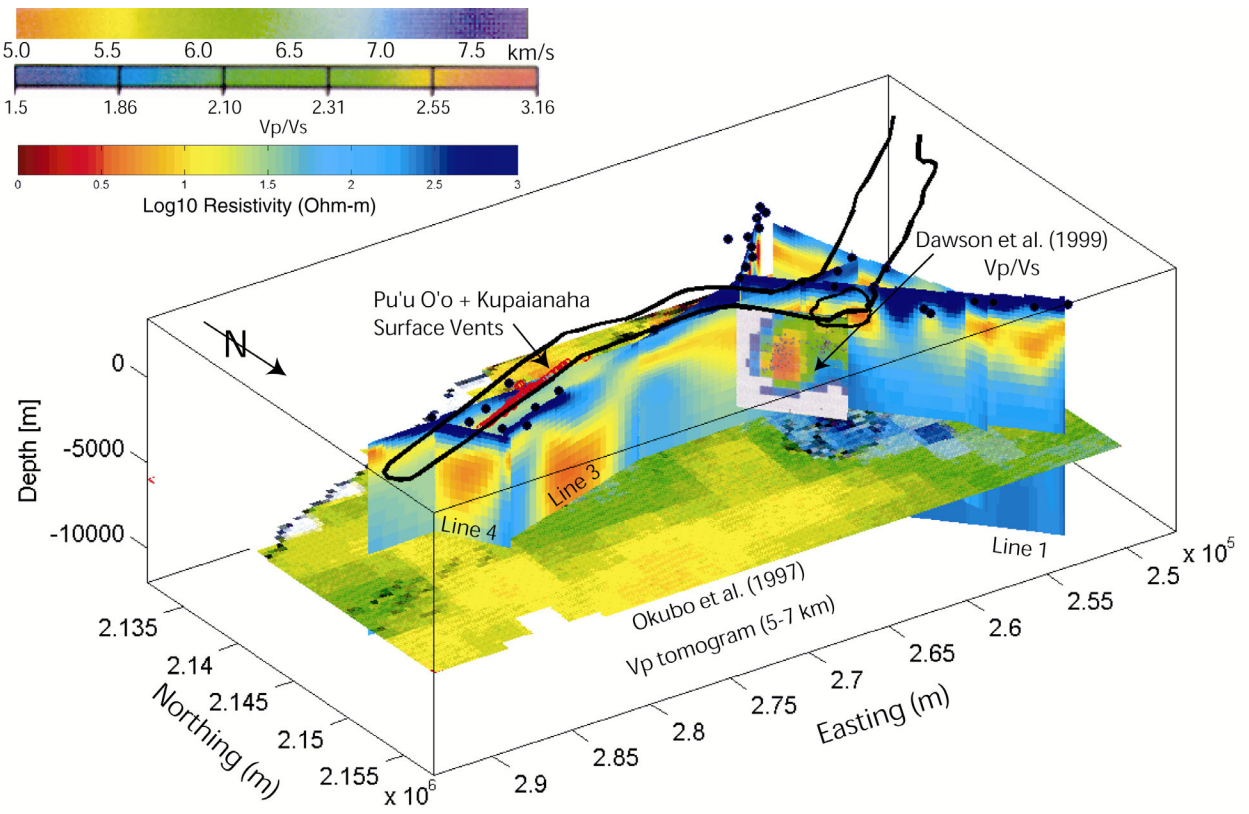

Hoversten et al., Figure 13